# Exploring the Application of SEBS for Precision Agriculture: Plant Scale Vineyard

MILAD MAHOUR
February, 2013

SUPERVISORS:
Prof. Dr. Ir. A. Stein
Dr. M.A. Sharifi

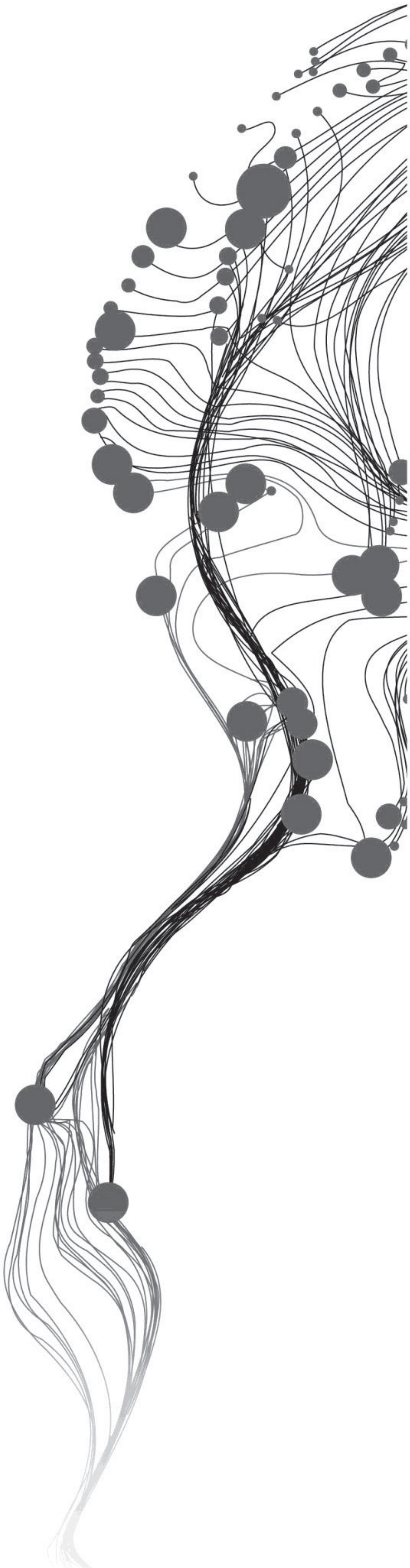

# Exploring the Application of SEBS for Precision Agriculture: Plant Scale Vineyard


MILAD MAHOUR

Enschede, The Netherlands, February, 2013



Thesis submitted to the Faculty of Geo-Information Science and Earth Observation of the University of Twente in partial fulfilment of the requirements for the degree of Master of Science in Geo-information Science and Earth Observation.

Specialization: Geoinformatics

SUPERVISORS:
Prof. Dr. Ir. A. Stein
Dr. M. A. Sharifi

THESIS ASSESSMENT BOARD:
Prof. Dr. Ir. M.G. Vosselman (Chair)
Dr. Ir. L. Kooistra (External Examiner, Wageningen UR)

# ABSTRACT

Precision Agriculture (PA) aims to use Remote Sensing (RS) techniques to provide the meaningful information at small scales for farmer and decision makers. Water deficit is one of the important issues of water resource managements with respect to the relevant factors to crop water requirement; to control the irrigation networks by farmer and who wants to make a decision. EvapoTranspiration (ET) is one of the important elements in order to determine the quantity of water requirements in agricultural fields.

Super Resolution Mapping (SRM) increases the resolution of classification result considering the resolution of the input image. During partitioning pixels of image to sub-pixels, Markov Random Field (MRF) as a contextual classification method that consider both spectral and spatial information of an image, try to overcome mixed pixels. Surface Energy Balance System (SEBS) is a remote sensing model to determine the actual ET with respect to the resolution of input RS data. Gram-Schmidt (GS) method as an image fusion technique applied to explore the possibility of integration of using SRM and the SEBS for assessing the crop water requirement.

We utilized high resolution satellite image to provide a smooth classification result using SRM based MRF. The optimum result of SRM is based on parameter estimation and the result compared to the reference data using digital aerial photo to assess the overall accuracy regarding kappa coefficient; satisfied the optimum result of SRM at rows within the field and plants within the row. Because of absence of providing potential ET from RS data, the maximum value of actual ET assumed as potential ET and compared to the result of potential ET based on Penman-Monteith and shows a less different between them. Finally, this approach has the potential to serve the farmer and decision makers to draw the outline of planning and strategies at irrigation networks for precision agriculture.



**Keywords:**
Precision agriculture, Remote sensing, Super resolution mapping, , Markov random field, Surface Energy Balance System, EvapoTranspiration, Water requirement

# ACKNOWLEDGEMENTS

I express my special grateful to my first supervisor Prof. Alfred Stein for his advice, help and continuous encouragement have contributed significantly to the completion of this study. I want to extend my appreciation to my second supervisor Dr. Ali Sharifi for his critical comments and advice that enhance this work. My very special thanks go to Dr. Valentyn Tolpekin for his kindly supporting me during this research. Thank you!

I would like to sincerely thank Miss Fakhere Alidoost and Saj GeoInformation System Company to provide me data sets. Special thanks to Mr. Ahmadi and Provincial Jihad-e-Agriculture of Ghazvin for providing the high resolution data (Ultracam and Geoeye). I would like to thank Dr. Markus Gerke for his trust and support in my work. I wish to thank Mr. Gabriel Parodi for his dedicated guidance.

I want to thank Dr. Ali Abkar and Dr. Kourosh Khoshelham for their support.

My deep appreciation goes to Mr. Mehdi Poor and Miss Eshraghi for their emotional support during this work and living in the Netherlands.

Finally, the love of my life my loving mother *Fariba* and my father *Jamshid*, thank you for giving me this life. Thank you for giving me a stable mind to think and work for science. Because of you I am standing here. I am thankful to you for all what you have done for me.


**.....This work dedicated to my family.....**

# TABLE OF CONTENTS


1. Introduction ........ 1
   1.1. Motivation and problem statement ........ 1
   1.2. Research identification ........ 2
   1.3. Research approach ........ 2
   1.4. Structure of thesis ........ 4
2. Literature review ........ 5
   2.1. Land cover classification ........ 5
   2.2. Mixed pixel and spectral unmixing ........ 5
   2.3. Super resolution mapping ........ 5
   2.4. Markov random field ........ 6
   2.5. Surface Energy Balance System ........ 6
   2.6. Image fusion ........ 7
3. Study area and materials ........ 9
   3.1. Study area ........ 9
   3.2. Satellite data ........ 9
   3.3. UltraCam digital aerial photo ........ 11
   3.4. Meteorological data ........ 12
   3.5. Software ........ 13
4. Methods ........ 15
   4.1. Super resolution mapping based on Markov random field ........ 15
   4.2. Crop water requirement ........ 19
   4.3. Image fusion for integration of actual ET and NDVI ........ 22
   4.4. Validation ........ 22
5. Results ........ 25
   5.1. SRM result from the GeoEye satellite image ........ 25
   5.2. Daily ET result from the Landsat 5 TM satellite image ........ 28
   5.3. Image fusion between actual ET and NDVI maps ........ 29
   5.4. Application of SRM and SEBS for precision agriculture ........ 30
6. Discussion ........ 33
7. Conclusion and recommendations ........ 37
   7.1. Conclusion ........ 37
   7.2. Recommendations ........ 38
   7.3. Future work ........ 38

# LIST OF FIGURES

Figure 1.1: Schematic Diagram of the proposed method for extracting individual plants................................3
Figure 1.2: Schematic diagram of applying image fusion using the SEBS and NDVI for actual ET..............3
Figure 3.1: Study area, Source: Google Earth..........................................................................................9
Figure 3.2: GeoEye satellite image of area of interest A) Panachromatic image with 0.5 $m$ resolution B) RGB color composite of multispectral bands with 2 $m$ resolution C) NIR color composite of multispectral bands with 2 $m$ resolution ..................................................................................................10
Figure 3.3: Landsat 5 TM image at area of interest A) RGB color composite B) NIR color composite .....11
Figure 3.4: UltraCam digital aerial photo of study area.........................................................................12
Figure 4.1: Different orders of neighbourhood system on the lattice of regular site r, Source: (Tso and Mather, 2009) ......................................................................................................................................16
Figure 4.2: Divided rows in A) GIS layer, B) GeoEye image, C) UltraCam digital aerial photo ..................19
Figure 4.3: Creating blocks for each plant A) GeoEye panchromatic image B) Reference polygons in the aerial photo..........................................................................................................................................19
Figure 4.4: Three input data sets for the SEBS ......................................................................................20
Figure 4.5: Reference polygons in digital aerial photo for assessing the result of SRM ...........................23
Figure 5.1: MLC result of panchromatic and multispectral images of the GeoEye data................................25
Figure 5.2: The result of SRM based MRF for the subset with S=4, $T0$=3, $Tupd$=0.9, λ=0.9 and $\lambda pan$=0.4 ......................................................................................................................................26
Figure 5.3: Result of SRM based MRF from row number 11 to row number 21 ...........................................27
Figure 5.4: The result of SRM for individual plants in row number 16 ........................................................28
Figure 5.5: The result of retrieval actual daily ET based on the SEBS around the area of interest..............29
Figure 5.6: Result of (C) image fusion between (B) actual ET image and (A) NDVI image using the GS method .................................................................................................................................................29
Figure 5.7: SRM result of (A) a row and (B) three individual plants for allocating actual ET.......................30
Figure 5.8: Combination of SRM result with NDVI for row number 18 and three plants of row number 16..........................................................................................................................................................31

# LIST OF TABLES

Table 3.1: Description of the spectral bands and ground resolution of GeoEye ........................................... 10
Table 3.2: Description of spectral bands and ground resolution of Landsat 5 TM........................................ 11
Table 3.3: Description of the spectral bands and ground resolution of UltraCam aerial photo .................. 12
Table 3.4: The ground meteorological data (Source: the Ghazvin weather station in Iran)........................... 13
Table 5.1: Optimum parameters of SRM based MRF......................................................................................... 25
Table 5.2: Result of actual ET in row number 18 and three individual plants in row number in row 16 ... 30
Table 5.3: NDVI value for row number 18 and three individual plants in row number 16 .......................... 31

# 1. INTRODUCTION

## 1.1. Motivation and problem statement

Precision Agriculture (PA) includes integration of using advanced technologies in Geomatics science such as Global Positioning System (GPS), Geospatial Information System (GIS) and Remote Sensing (RS). Many studies have been done regarding precision agriculture and remote sensing during last two decades. Because , there is an uncertainty whereas to adopt a policy of available techniques on the agricultural area (Zhang et al., 2002). Use of remote sensing technologies in PA applications allows farmers to manage their farm products as a maximization cost-benefit ratio in terms of field variation more than using traditional techniques (Brisco et al., 1998). The results of water consumption for various land cover types play a predominant role in PA regarding appropriate water resource management for decision makers (Wu et al., 2012). Nowadays, water deficit is one of the major impacts of improper water resource management in agricultural areas. There are many factors considering the absence of knowledge about the water requirement in many agricultural fields. One of the important elements regarding this issue is to determine the amount of crop EvapoTranspiration (ET). In the agricultural irrigation systems, water is used to provide enough water for plant ET; that is the actual crop water requirement. There are many factors that indicate how much water will be lost during the ET such as crop type, vegetation cover and climate factors. Two types of ET can be distinguished, Potential EvapoTranspiration (PET) and Actual EvapoTranspiration (AET). SEBS (Surface Energy Balance System) (Su, 2002), contains integration many tools for determining physical properties of the land surface and it can assess AET (Wang et al., 2008). It requires three types of data input information including land surface properties from RS data, meteorological data and SW (Short Wave) and LW (Long Wave) radiation from direct measurement or model output (Wang et al., 2008). Some users, e.g. decision makers and farmers who want to manage their farms as of water plan irrigation, need to know the water requirements of each tree individually.

The most important aim of image processing of Remotely Sensed (RS) data is extracting useful information from satellite data. These data need to be analysis to obtain useful information. The general approach for analyzing RS data is classification. Image classification method assigns labels to each pixel considering spectral behaviuor in order to translate the continuous variability of image data into map pattern that provide meaningful information for end users. Image with coarser resolution reduces the characteristics of an object and it leads to mixed pixels which are not quantified as of hard classification technique (Muad and Foody, 2010). Unlike fine spatial resolution imagery, coarse spatial resolution imagery consists of mixed pixels which are include several classes while a pure pixel has only a single class (Muad and Foody, 2010). There are several satellite images which provide a fine spatial resolution imagery in RS system such IKONOS, SPOT5, QUICKBIRD with both multispectral and panchromatic images that contains finer spatial resolution (Muad and Foody, 2010). Using Very High Resolution (VHR) images aims to extract accurate objects individually but, there are some limitation in this issue based on restricted spectral information satellite sensors and their spatial resolutions (Tolpekin et al., 2010).

The aim of this research is to achieve accurate information on plant scale vineyard from coarse spatial and spectral resolution of images. In addition, individual plants will be extracted by using Super Resolution Mapping (SRM) technique based on Markov Random Field (MRF) at finer resolution. In order to achieve a finer spatial resolution by means of obtaining much spatial information in classification techniques, it is necessary to perform down-scaling method from the coarser resolution to finer resolution (Sepehri, 2011). The main objective of using SRM technique is to detect and identify rows within the field and plants within the rows in order to execute a hard classification technique. SRM provides classification maps at finer resolution from coarser resolution compare to initial input image (Atkinson, 2009). The other problem is related to the coarse resolution images using the SEBS to retrieve actual ET. Fusion techniques will be proposed to overcome this issue.

## 1.2. Research identification

The main research objective is to explore the possibility of assessing crop water requirement using SRM and application of SEBS. The focus will be more on the application of SRM to provide relevant input data to be used for down-scaling the lower resolution result to the higher resolution.

### 1.2.1. Research objectives

The objectives of this research are:

- To estimate the actual and potential EvapoTranspiration at plant scale vineyard by using SRM and the application of SEBS.
- To assess applicability of integrated SEBS and SRM.
- To determine the quantity of water requirements at plant scale using different fusion techniques.

### 1.2.2. Research questions

The research questions of this research are:

1. Which satellite images are appropriate as a spatial resolution to support SRM for extracting information on plant scale vineyard?
2. What could be the role of SRM at plant scale information for vineyard?
3. How to extract information of indivitual plants of vineyard with SRM?
4. How to validate the result of SRM?
5. How to integrate SEBS and SRM?

### 1.2.3. Innovation aimed at

The novelty of this research is the application of SRM to extract plants information for supporting precision agriculture.

## 1.3. Research approach

The aim of this research is utilizing contextual MRF based on SRM in order to sub-divide image pixels to obtain finer spatial resolution. This study will focus on SRM based on MRF at the plant scale vineyard in order to identify each row and extract individual plants of grape trees. Figure 1.1 illustrates the flowchart that shows the suggested SRM based MRF methodology for this research.

The general methodology of this research divides in three steps. In the first step, the SRM based on MRF supposes to detect rows and plants. Furthermore, assessing the result will be considered to decrease uncertainty. The second step, use the SEBS to determine the ET for plant scale vineyard for supporting precision agriculture. In last step (Figure 1.2), image fusion technique utilizes to integrate the SEBS and SRM result.

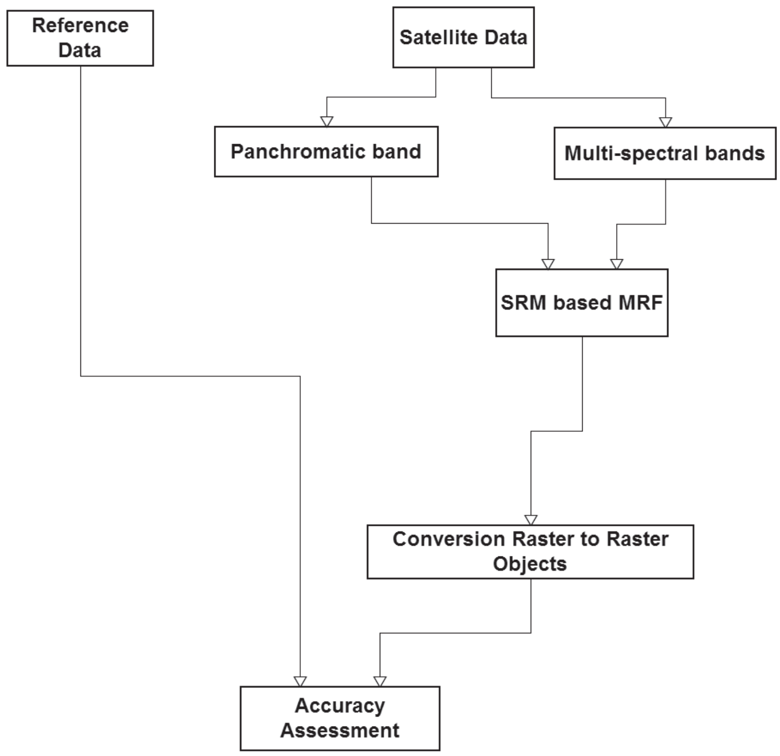


Figure 1.1: Schematic Diagram of the proposed method for extracting individual plants

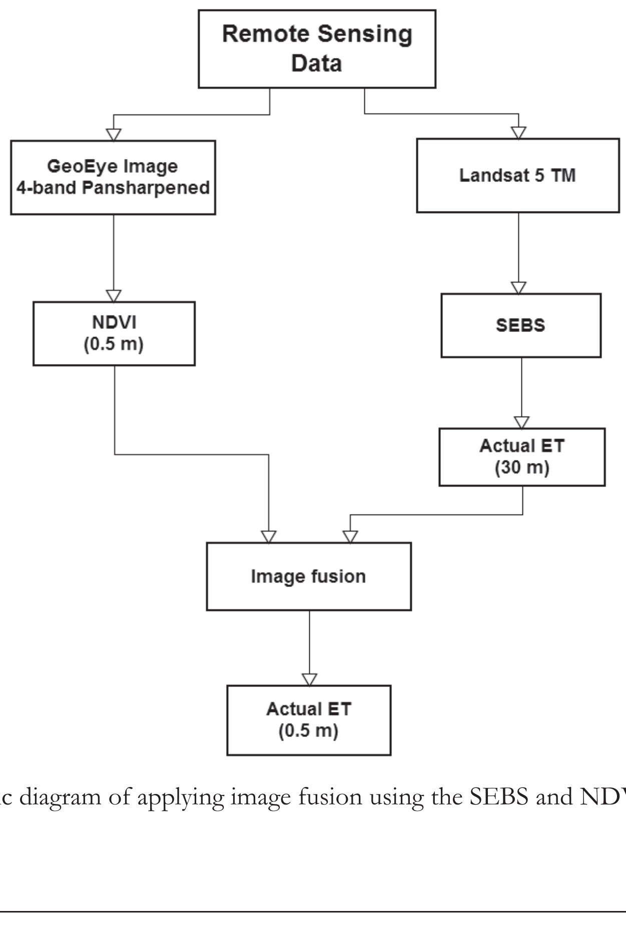


Figure 1.2: Schematic diagram of applying image fusion using the SEBS and NDVI for actual ET

### 1.4. Structure of thesis

The thesis established in seven chapters. The chapter one presents the motivation and problem statement of this study, objectives, research questions and research approach of this research. The second chapter demonstrates overall review regarding alternative land cover classification methods, SRM and Surface Energy Balance System (SEBS) and image fusion technique. Chapter three explains the proposed methodology of research approaches. Chapter four presents a brief introduction of the study area and remote sensing data sets. Chapter five illustrates the result of SRM based MRF and retrieval daily ET regarding possibility of integration between the SEBS and SRM result. Chapter six discusses how the result analyzed and how they can be linked. The last chapter makes the conclusion and recommendation for promotion researches.

# 2. LITERATURE REVIEW

## 2.1. Land cover classification

The most important aim of image classification of Remotely Sensed (RS) data is extracting useful information from satellite data. These data need to be analysis to obtain useful information. The general approach for analyzing RS data is classification that includes diverse methods which have many advantages and disadvantages. Image classification method assigns labels to each pixel considering spectral behaviour in order to translate continuous variability of image data into map pattern. This thematic map provides meaningful information for end users. Image classification methods have done using spectral bands in order to assign an appropriate land cover classes to each pixel. Generally, image classification methods comprise to two main methods which are supervised and unsupervised classifications. Supervised classification methods use training pixels with respect to class separability that defined by users. Taking training pixels needs experience in RS data and visiting field work. Unsupervised classification methods use spectral range for assigning label classes to generate a thematic map (Richards, 2012). Supervised classification methods identified as parametric and non-parametric classification method. Maximum Likelihood Classification (MLC) is the most common supervised classification (Richards, 2012) as a parametric method which uses statistical parameters such as mean and covariance to allocate label class to each pixel. It means that the result of classification is sensitive to taking training pixels (Mahour and Abkar, 2012) . The result of MLC as the thematic map leads to the noisy result as mixed pixels. Support Vector Machine (SVM) is one of non-parametric classification method that has used in many researches recently. Non-parametric methods no need statistical parameters for calculation pixel values considering training pixels. Classification methods contain diverse errors which are related to mixed pixels, sensor effects, atmospheric effects and radiometric overlap between land cover objects (Abkar and Fatemi, 2004). To improve these errors some methods were performed by related works such as object-based and knowledge-based classification (Abkar et al., 2000) by using extra information at the object level. These methods deal to reach high evaluation but because of lacking reference data they cannot implement correctly.

## 2.2. Mixed pixel and spectral unmixing

The problem of land cover classification is related to the noisy result as mixed pixels. Identifying mixed pixels in boundary of two classes has a main role in classification results. It means that during satellite sensor scanning as Instantaneous Field of View (IFOV), one pixel size as spatial resolution of an image can have more than one class with respect to spectral reflectance of land cover on the earth (Foody, 2006). Fisher (1997) introduced four types of mixed pixels such as boundaries are among the more than one mapping unit, integration between phenomena, linear sub-pixel objects and small sub-pixel objects. Soft classification or sub-pixel classification classified mixed pixels in different classes using membership value (Haglund, 2000). Spectral unmixing is a technique that used fraction of each mixed pixel to assign the number of classes to each pixel (Foody, 2006). Moreover, this approach resolves the spectral mixture problem.

## 2.3. Super resolution mapping

Super Resolution Mapping (SRM) is a technique that partitioning pixel into smaller ones in order to achieve high spatial resolution from coarser imagery. SRM has been proposed using diverse algorithms such as Hopfield neural networks, genetic algorithm, neural network predicted coefficients, knowledge-based procedure and linear optimization (Sepehri, 2011). All abovementioned techniques take a coarse spatial image input (Muad and Foody, 2010). Tatem et al. (2001) developed SRM with Hopfield neural network to minimize energy as a tool for fuzzy classification result. After that, they applied their algorithm on Landsat TM data to exhibiting higher accuracy compare to traditional algorithms but not for complicated features (Tatem et al., 2003). Verhoeye and De Wulf (2002) proposed the application of linear optimization technique for sub-pixel mapping. Their algorithm had restriction as spatial dependency of objects of smaller pixels (Sepehri, 2011). Mertens, et al. (2003) applied the genetic algorithm in SRM and achieved the precise result. Unlike fast computation, some parameters have been found in genetic algorithm as of disadvantage (Sepehri, 2011). Boucher and Kyriakidis (2006) implemented the geostatistical method as of indicator kriging in SRM to evaluate spatial variety of classes. After two years, they utilized the training image for variogram model as of prior information. Kasetkasem, et al. (2005) introduced Markov Random Field (MRF) based on SRM for the first time. In their paper, MRF used to model spatial dependency of each pixel by the use of statistical correlation of neighboring pixels. They found that including MRF in SRM generate classified map with a few misclassified pixels and also their result on land cover map was smoother (Kasetkasem et al., 2005). Tolpekin, Stein (2009) used MRF based on SRM method of Kasetkasem, et al.(2005) to show the class separability by introducing smoothness parameters as of prior and conditional energy. They pointed out the result of SRM related to several parameters such as smoothness parameters, class separability and scale factor (Tolpekin and Stein, 2009). Lopez (2012) proposed MRF based on SRM for identification of urban trees in very high resolution images considering energy function, spatial smoothness prior and conditional probability. He achieved acceptable result for detecting tree crowns in residential area and concluded that the method decreases influence of spatial resolution in terms of large class spectral variance in input images (Ardila Lopez, 2012).

### 2.4. Markov random field

Markov Random Field (MRF) is a contextual and probabilistic method that has been used in image segmentation and image restoration (Tso and Mather, 2009). Context means spectral, spatial and temporal attributes. The possibility use of context leads to correct the errors, omit the vagueness and cover again missing information (Li, 2009). MRF for supervised and unsupervised segmentation methods was developed by Hu and Fahmy (Hu and Fahmy, 1992). Sarkar (2002), compare the result of MRF as energy minimization with Maximum Likelihood Classification (MLC) and observed that the result of MRF was better than MLC in different samples. Tso and Oslen (2005) developed MRF based multi-scale fuzzy for image classification. They utilized IKONOS image consists of multispectral and panchromatic images and estimate the optimum parameters using probability histograms.

### 2.5. Surface Energy Balance System

Evapotranspiration is the important issue of water balance and it utilizes for irrigation network and agricultural land intuition (Ma et al., 2012a). Evapotranspiration comprises to two separate and simultaneous processes which are evaporation and transpiration. Evaporation is the process of losing transferred water from the soil and the process of losing water from the vegetation through the atmosphere. These two processes occupy simultaneously and they required a source of water, a source of energy and a slope of vapour (Kalma et al., 2008). The three mentioned requirements for determining evapotranspiration extensively classified in three methods as mass budget methods, energy budget methods and methods base on atmospheric turbulence and mean profile measurements (Kalma et al., 2008). Kalma et al. (2008) pointed out the surface energy models are a solution of the surface energy budget. There are several models based on remote sensing and field observation measurements such as

the Surface Energy Balance Algorithm for Land (SEBAL) developed by Bastiaanssen et al. (1998) which uses the hot and cold points of satellite image to provide the empirical temperature difference equation. The Surface Energy Balance Index (SEBI) (Menenti and Choudhury, 1993), the Simplified Surface Energy Balance Index (S-SEBI) (Roerink et al., 2000), Mapping Evapotranspiration with Internalized Calibration (METRIC) (Allen et al., 2007).
The SEBS (Su, 2002) from the SEBI components was presented to estimate atmospheric turbulent fluxes, the evaporative fraction and actual ET using satellite image data and meteorological information at an appropriate scale (Su, 2002). SEBS includes a toolbox for determining physical parameters of land surface such as albedo, land surface emissivity and land surface temperature from spectral radiance and reflectance measurements of satellite earth observation data. Ma et al. (2012b) retrieved the actual ET from the Landsat 5 TM by the use of SEBS for irrigation area. They used satellite images of different years for obtaining daily ET and then compared their result with ground measurements data and found that deriving ET from the SEBS are highly close to the field measurements.

## 2.6. Image fusion

Remote sensing satellite data provide finer spectral and coarser spatial resolution or lower spectral and higher spatial resolution with respect to optical sensor systems (Ha et al., 2012). Considering use of finer spectral and spatial resolution images, image fusion techniques have been proposed in many applications for irrigation management systems in precision agriculture. Wansook (2012) observed that image fusion methods have not potentially utilized in achieving finer resolution evapotranspiration images in application of precision agriculture. Thomopoulos (1990) first introduced the data fusion as an arranged seminar by NASA. Data fusion comprises of three levels from lowest to highest data viewing such as pixel level, feature level and decision level (Luo and Kay, 1992). In remote sensing images, data fusion has utilized as the pixel level in raster formats (Zhuang et al., 2011). Image fusion can be applied for various application of image enhancements such as improving the result of classification (Pohl and Van Genderen, 1998). There are many research have been done regarding image fusion techniques using two different satellite sensors. Most of these studies considering the merging Landsat Thematic Mapper (TM) and System Poourl' Observation de la Terre (SPOT) satellite images (Ha et al., 2012).
There are different methods as the data fusion methods in remote sensing image analysis such as Principal Component Spectral Sharpening (PCSS), IHS (Intensity, Hue, Saturation), Color Normalized (Broevy) Sharpening, Gram-Schmidt Spectral Sharpening (GS) and wavelet fusion. These methods use different algorithm but, the result of final fused images contains a subsequent goal (Zhuang et al., 2011). Image fusion merges a low resolution color or multispectral image with a high resolution image by the use of resampling the lower resolution image to the high resolution image (Vrabel, 1996). Zhuang et al. (2011) utilized different methods for image fusion and observed that extracted information from NDVI by using the GS method had better results in remaining spectral and brightness information compare to other methods.

# 3. STUDY AREA AND MATERIALS

In this research, various remote sensing data sets will be utilized in order to apply the proposed methodology. Remote sensing data include GeoEye satellite image, UltraCam digital aerial photo and Landsat 5 TM image. This chapter presents a brief introduction of remote sensing data and explanation of the study area.

## 3.1. Study area

The study area is located in Sharifabad as a town in the center of the Ghazvin province in the north-west of Iran. Geographical information on the area is 36°11'21" N, 50°13'19" E. The area of open homogeneous land planted with grape trees as an industrial agricultural field (Figure 3.1). The area consists of grape trees as rows and length of each row is approximately 40 $m$. The distance between each row is 3 $m$ and height of the plants are 2 $m$ respectively. In this research, from this field GeoEye satellite image, UltraCam digital aerial photo and Landsat 5 TM satellite image utilize for performing the proposed methodology.

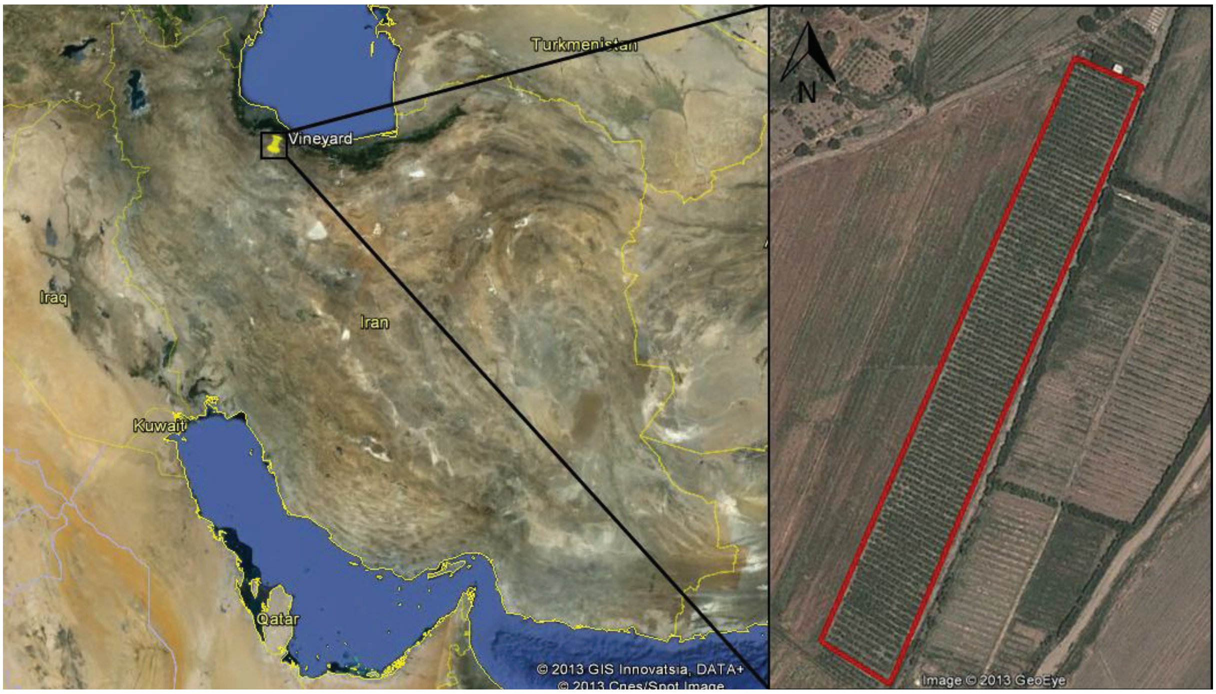


Figure 3.1: Study area, Source: Google Earth

## 3.2. Satellite data

### 3.2.1. GeoEye -1 image

GeoEye-1 is a high resolution satellite image which was launched by U.S. company GeoEye in September 2008. It has taken highest ground resolution images as a civilian space observation system. GeoEye-1 is capable to acquire image data with 0.41 $m$ in panchromatic and 1.65 $m$ in multispectral resolution and because of U.S. government limitation the image provided to 0.5 $m$ resolution in panchromatic band for all customers (Dowman et al., 2012). GeoEye provides image products as simultaneous panchromatic and multispectral (pan-sharpened) product, only panchromatic and multispectral bands separately. Table 3.1

illustrates the description of the spectral and spatial information of panchromatic and multispectral bands of GeoEye.

Table 3.1: Description of the spectral bands and ground resolution of GeoEye

| Band Number | Bandwidth ($nm$) | Ground Resolution ($m$) | Description of Wavelength band |
|---|---|---|---|
| **Band 1** | 450 - 510 | 2 | Visible (Blue) |
| **Band 2** | 510 – 580 | 2 | Visible (Green) |
| **Band 3** | 655 – 690 | 2 | Visible (Red) |
| **Band 4** | 780 – 920 | 2 | Near Infra Red |
| **Pan** | 450 - 800 | 0.5 | Panchromatic |

The GeoEye satellite image data as of four bands pan-sharpened, multispectral and panachromatic images used in Ghazvin province that were collected on June 19, 2011. The image data was projected in Universal Transfer Mercator (UTM) with the standard spheroidal reference surface WGS 84. Figure 3.2 displays different color composite of the multispectral and the panchromatic images of area of interest.

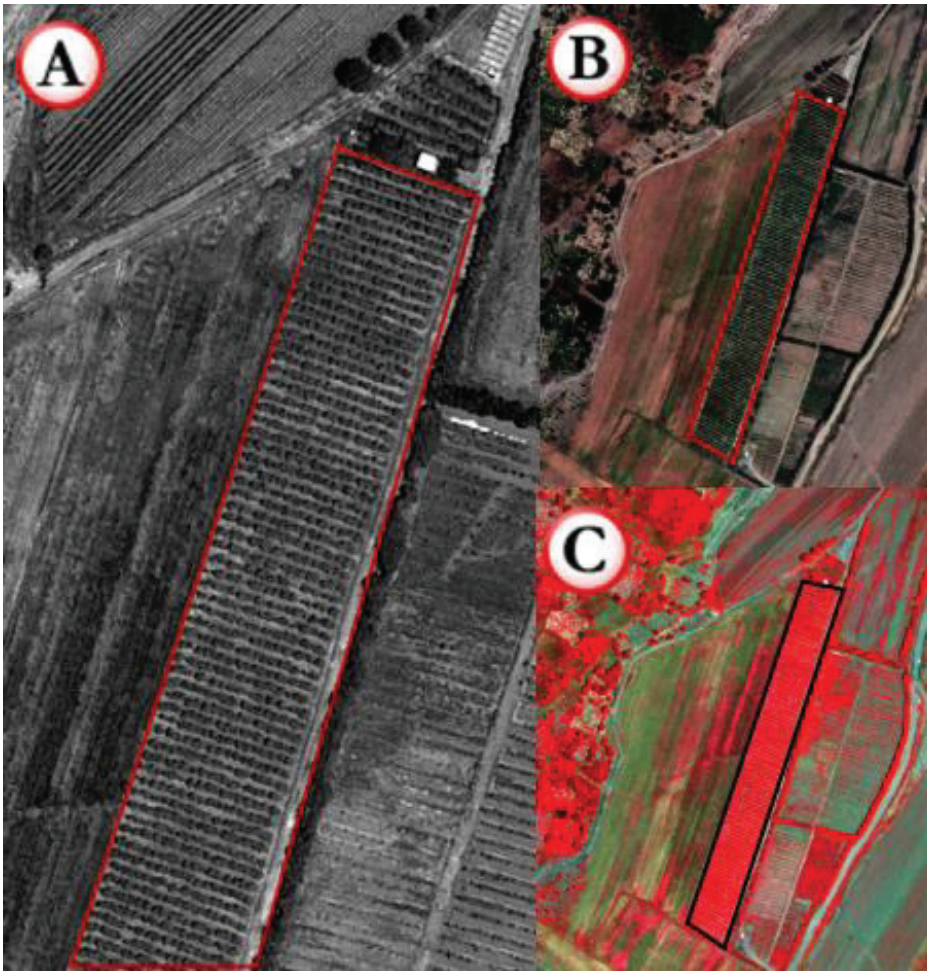


Figure 3.2: GeoEye satellite image of area of interest A) Panachromatic image with 0.5 $m$ resolution B) RGB color composite of multispectral bands with 2 $m$ resolution C) NIR color composite of multispectral bands with 2 $m$ resolution

#### 3.2.2. Landsat 5 TM image

Landsat 5 was launched by NASA in March 1984. It includes MSS (Multispectral Scanner System) and TM (Thematic Mapper). In August 1996, the MSS instrument was turned off but the TM instrument is still working after 28 years. In this study, the Landsat 5 TM image data used from the U.S. Geological Survey (USGS: http://glovis.usgs.gov) company on August 1, 2011 (Figure 3.3). The image contains seven multispectral bands of visible, near infrared and middle infrared with 30 $m$ ground resolution and a thermal band with 120 $m$ ground resolution for performing the SEBS methodology. Table 3.2 indicates the description of spectral bands of Landsat 5 TM image data.

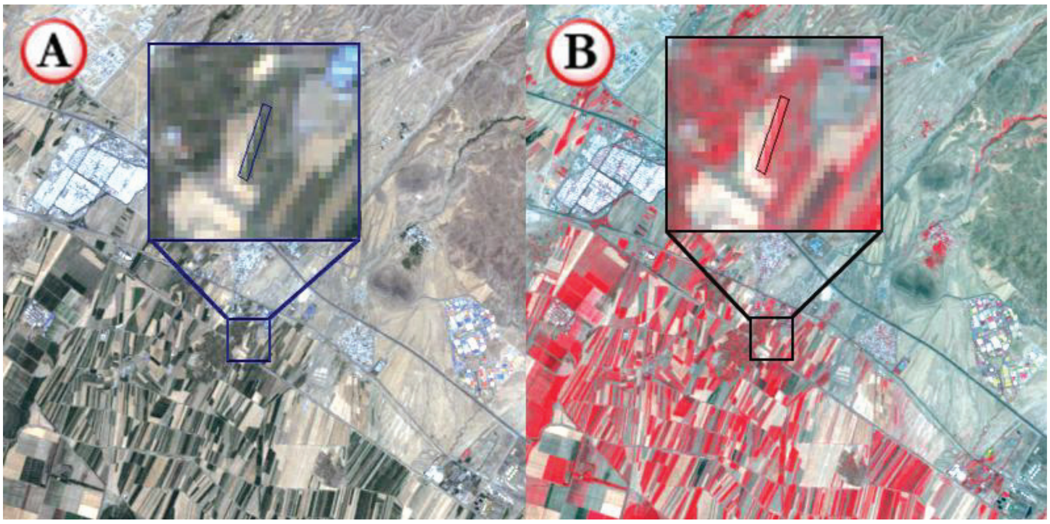


Figure 3.3: Landsat 5 TM image at area of interest A) RGB color composite B) NIR color composite

Table 3.2: Description of spectral bands and ground resolution of Landsat 5 TM

| Landsat 5 TM | Wavelength ($\mu m$) | Resolution (Meter) | Description |
|---|---|---|---|
| **Band 1** | 0.45 – 0.52 | 30 | Blue |
| **Band 2** | 0.52 – 0.60 | 30 | Green |
| **Band 3** | 0.63 – 0.69 | 30 | Red |
| **Band 4** | 0.76 – 0.90 | 30 | Near Infrared |
| **Band 5** | 1.55 – 1.75 | 30 | Mid Infrared |
| **Band 6** | 10.40 – 12.50 | **30*** | Thermal Infrared |
| **Band 7** | 2.08 – 2.35 | 30 | Mid Infrared |

* Landsat 5 TM consist of seven spectral bands and the resolution of bands 1-5 and band 7 is 30 $m$. The thermal infrared band (band 6) is collected 120 $m$ resolution but, as a level 1 product it was resampled to 30 $m$ resolution (http://eros.usgs.gov/Find_Data/Products_and_Data_Available/TM).

### 3.3. UltraCam digital aerial photo

The Microsoft UltraCam group has been providing the most advance technological UltraCam photogrammetric digital aerial mapping cameras since 2004. The UltraCam products offer customers an alternative technology compare to using traditional film aerial technology. In this research, the UltraCam digital aerial photo was taken on July 17, 2012 with 14 $cm$ ground resolution at visible and near infrared multispectral range. The digital photo was taken by Vexcel Imaging and the camera model is UltraCamXp.

Figure 3.4 shows the area of interest in different color composite of UltraCam photo. Table 3.3 indicates the description of spatial and spectral information of the UltraCam digital aerial photo.

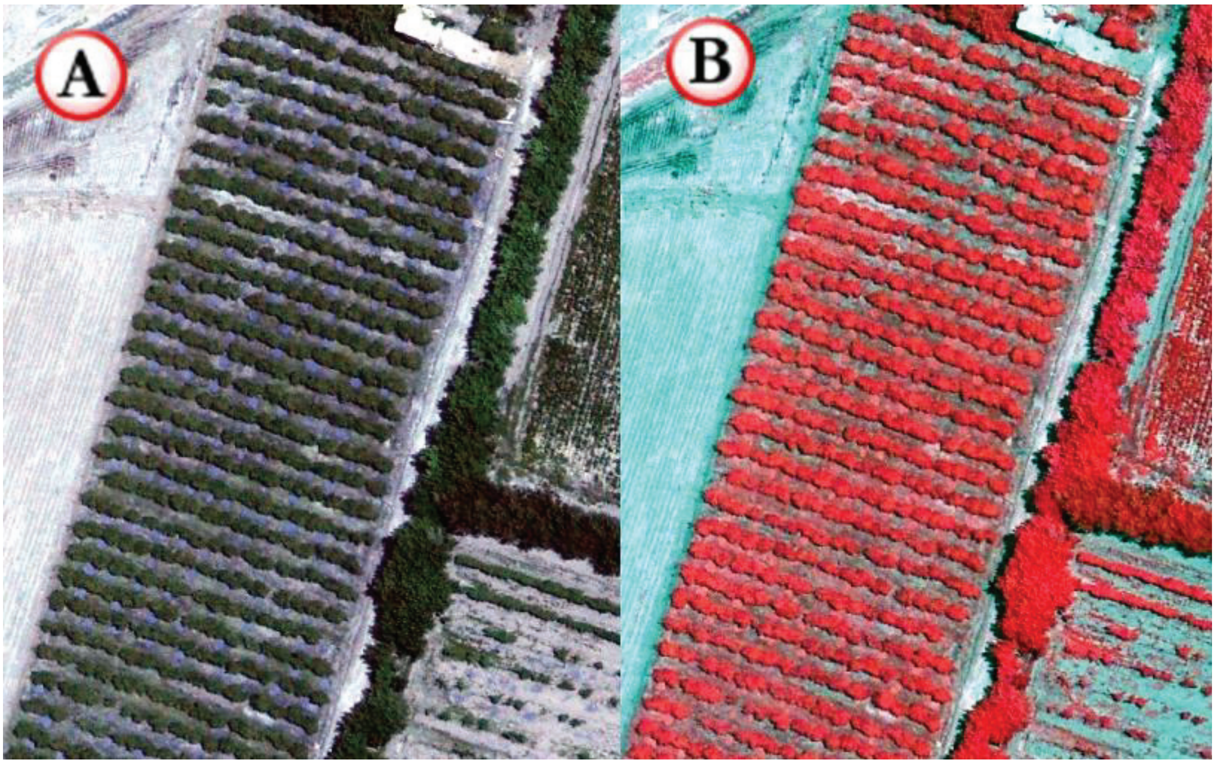


Figure 3.4: UltraCam digital aerial photo of study area
A) RGB color composite with 14 $cm$ ground resolution
B) NIR color composite with 14 $cm$ ground resolution

Table 3.3: Description of the spectral bands and ground resolution of UltraCam aerial photo

| Band Number | Bandwidth ($nm$) | Ground Resolution ($cm$) | Description of Wavelength band |
|---|---|---|---|
| **Band 1** | 400 – 600 | 30* | Visible (Blue) |
| **Band 2** | 480 – 600 | 30* | Visible (Green) |
| **Band 3** | 580 – 720 | 30* | Visible (Red) |
| **Band 4** | 620 - 1000 | 30* | Near Infra Red |

- **Digital Aerial Photo Pre-processing***

In order to make an accurate reference, the digital aerial photo was geometrically corrected (orthorectified) and georeferenced by the use of ERDAS Imagine and ArcGIS software respectively. The ground control points were extracted from the GeoEye satellite image. After orthorectifying the pixel size as ground resolution changed from 14 $cm$ to 30 $cm$.

### 3.4. Meteorological data

The weather data was collected by the Ghazvin weather station in Iran during a day of August 1, 2011 for utilizing the SEBS methodology. Table 3.4 shows the recorded weather data. In this table, time of recording data are based on Greenwich Mean Time (GMT) and the unit of each element such as wind speed is $m\,s^{-1}$, temperature is centigrade, sunshine hours is hours (decimal), radiance is $Kj\,m^{-2}$, rainfall is $mm$, air pressure is $mbar$ and humidity is shown as percentage. Moreover, the time between 6 to 9 was used because of acquiring time of Landsat 5 TM data at 7 a.m. Furthermore, the sign (-) in the table means there is no any record at that time.

Table 3.4: The ground meteorological data (Source: the Ghazvin weather station in Iran)

| Year | Month | Day | Hour | Wind Orientation | Wind Speed | Maximum Temperature | Minimum Temperature | Sunshine Hours | Rainfall | Humidity | Air Pressure | Radiance |
|---|---|---|---|---|---|---|---|---|---|---|---|---|
| 2011 | 8 | 1 | 0 | 60 | 1 | - | - | - | - | 25 | 868.8 | - |
| 2011 | 8 | 1 | 3 | 0 | 0 | - | 17 | - | - | 39 | 868.8 | - |
| 2011 | 8 | 1 | 6 | 130 | 3 | - | - | - | 0 | 17 | 868.8 | - |
| 2011 | 8 | 1 | 9 | 100 | 2 | - | - | - | - | 10 | 868.8 | - |
| 2011 | 8 | 1 | 12 | 210 | 3 | - | - | - | - | 10 | 868.8 | - |
| 2011 | 8 | 1 | 15 | 0 | 0 | 37.4 | - | - | - | 20 | 868.8 | - |
| 2011 | 8 | 1 | 18 | 0 | 0 | - | - | 12.7 | - | 31 | 868.8 | 2848 |
| 2011 | 8 | 1 | 21 | 0 | 0 | - | - | - | - | 34 | 868.8 | - |

The Ghazvin weather station is located in the north of the Ghazvin city in Ghazvin province which has approximately 17 $km$ distance from the study area. The geographical information of the weather station is 36°15'00" N, 50°30'00" E.

## 3.5. Software

In this study, there were many different softwares utilized for applying the proposed methodology.

- **ArcGIS**

ArcGIS is a GIS software that is developed by ESRI as U.S. Supplier Company to provide GIS software. ArcGIS tools were employed for co-registering remote sensing datasets and obtaining meaningful results in this research.

- **ENVI**

ENVI is geospatial image analysis software that contains efficient tools for image processing. In this study ENVI was used for preprocessing of remote sensing images, extracting subsets of area of interest, sensor calibration, extract basic statistics of training sets from the GeoEye image and calculating input data for SEBS such as albedo and emissivity.

- **ERDAS Imagine**

ERDAS Imagine is a remote sensing and a GIS software package with a raster graphic editor for geospatial applications. ERDAS embraces a professional toolbox which is Leica Photogrammetry Suite (LPS) to ortho-correct digital aerial photos.

- **ILWIS**

ILWIS (Integrated Land and Water Information System) is a vector and raster processing software that is developed by faculty ITC, university of Twente. It includes the SEBS tool and all procedure of data preprocessing such as atmospheric correction and computes land surface temperature, land surface emissivity, land surface albedo and brightness temperature. In the process of running SEBS in this study, it is used for atmospheric correction and performing the SEBS using Landsat 5 TM image data and integration of ground meteorological data.

- **R Software**

R software (CRAN) is an open source programming language for calculating statistics and creating different graphics. In this research it is used for executing SRM with MRF on the GeoEye satellite image and assessing the result using the UltraCam digital aerial photo.

# 4. METHODS

## 4.1. Super resolution mapping based on Markov random field

Detecting rows and individual plants in industrial agricultural fields from RS data requires spatial and spectral information. Traditional classification methods such as Maximum Likelihood Classification (MLC) as a pixel-based method cannot consider spatial characteristics of RS data and just consider the spectral behaviour of multispectral bands. In this research, SRM based on MRF as a contextual and probabilistic classification method (Tso and Mather, 2009) applied in high resolution image to identifying rows and extracting individual plants in the plant scale vineyard for supporting precision agriculture applications. Super Resolution Mapping (SRM) increases the resolution of the classification result with respect to the resolution of the input image. The average of pixel values of the finer resolution image is the same as pixels inside the coarse resolution pixels (Tatem et al., 2001). By using SRM, pixels in the coarse resolution image partitioned to finer pixels to assigning class labels at the finer resolution image respectively with maximum spatial dependency (Atkinson, 2009). Markov Random Field (MRF) as a kind of probability theory models the spatial dependency to each pixel at the finer resolution image regarding statistical correlation of neighboring pixels (Kasetkasem et al., 2005).

Let $y$ be a coarse resolution image and $x$ be the classified image from fine resolution image and let $S$ be the scale factor between $y$ and fine resolution image. The number of pixels in the fine resolution image includes $SM \times SN$ dimension concerning the number of pixels have $M \times N$ dimension at the coarser resolution image. Therefore, each pixel in the coarse resolution image contains $S^2$ number of pixels in the finer resolution image. It is assumed that the finer spatial resolution image comprises pure pixels compare to mixed pixels which occupy at the coarser spatial resolution image (Kasetkasem et al., 2005). Hence, each pixel in the coarse resolution image can include more than one class. Each pixel in the fine resolution image represents as $a_{i|j}$, $i$ is identified as the pixels in the coarse resolution image (i.e., $i = \{1, \dots, M \times N\}$), and $j = \{1, \dots, S^2\}$, as the included pixels in the fine resolution image. Let $b_i$ , be the each pixel in the coarse resolution image as stated earlier. Finally the corresponding relation between $x$ and $y$ represents as a model which shows the degradation of each pixel of $b_i$ :

$$y(b_i) = \frac{1}{S^2} \sum_{j=1}^{S^2} \mathrm{x}(a_{i|j}) \tag{3.1}$$

By down-scaling each pixel of the coarse resolution image, the initial SRM map will be provided as a scale factor $S^2$, in the fine resolution image which are sub-pixels. During the down-scaling, the randomly labels assigned to each of these sub-pixels. However, there are no any correct class labels to all the sub-pixels. So, it is necessary to propose a method which renews the class level of sub-pixel correctly in initial SRM (Kasetkasem et al., 2005). In this research, MRF as a contextual classification method was utilized for finding the spatial dependency of each sub-pixel that produced from SRM. In this chapter, the following sections present the combination of SRM and MRF method.

### 4.1.1. Neighbourhood system

Let $K$as a site which contains $m$ number in which each random variable $x = \{x_1, \dots, x_m\}$ takes a label from label set $L$. Then $K$ can be identified as a set of sites (Li, 2009):

$$K = \{1, .., m\} \tag{3.2}$$

The image  with pixel $(i,j)$ and $M \times N$ dimension a rectangular lattice which is spatially regular is written as:

$$K = \{(i,j)|\ 1 \leq i,j \leq m\} \tag{3.3}$$

The sites in $K$ are corresponding to each other neighbours regarding a neighbourhood system. The neighbourhood system for $K$ is defined as:

$$N = \{N_r | \forall_r \in K\} \tag{3.4}$$

where $N_r$ is the set of sites which neighboring $r$. The relationship between neighbors contains the below properties:

1) A site is not neighboring to itself: $r \notin N_r$
2) The relationship between the neighbors is mutual: $r \in N_{\acute{r}} \leftrightarrow \acute{r} \in N_r$

Regarding the neighbourhood system in image analysis,  Li (2009) identified different type of ordering of neighbours. The first order neighbours of a pixel contains four pixels that share the border with pixel $r$. The second order neighbours of a pixel include four pixels that share corner boundaries with a pixel $r$, additionally. The higher order neighbours of a pixel can be extended in a similar way (Tso and Mather, 2009).

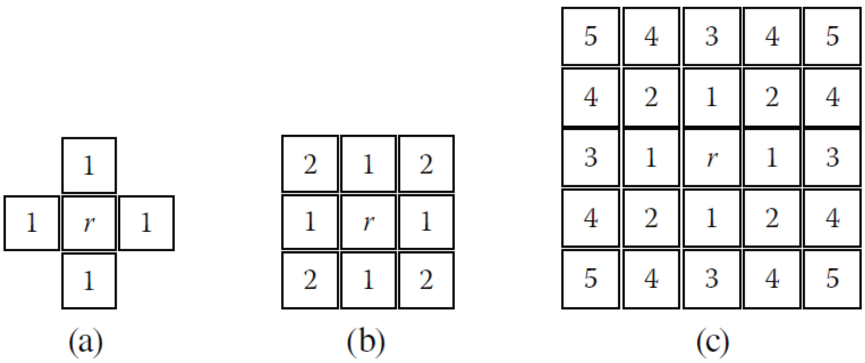

Figure 4.1:  Different orders of neighbourhood system on the lattice of regular site r, Source: (Tso and Mather, 2009)

The pixels of two-dimensional image $y$ include the sites as a rectangular lattice. The site $r = (i,j)$ contains four nearest neighbours as a first order neighboring system (Tso and Mather, 2009). There are three neighbours at the boundary side of image which consist of two neighbours at the corners. The scale factor in SRM as $S$ will be affected on neighbourhood system (Figure 4.1). Let $W_{size}$ as a awindow size, so the relation between scale factor and window size can be calculated as (Kassaye, 2006):

$$W_{size} = 2(S-1) + 1 \tag{3.5}$$

#### 4.1.2. Markov Random Field and Gibbs Random Field

During SRM, a contextual classification method which is Markov Random Field (MRF) is applied to overcoming mixed pixels with respect to both multispectral and panchromatic images as the spectral and spatial contextual information. There are various random field models which contain several methods of

labelling random variables. MRF is a model that takes the label set to the random variables from SRM with respect to spatial dependency of each pixel (Tso and Mather, 2009).
Let $x$ be a set of DN value with respect to each of pixel. The group $x$ is called random field. The label set $L$ is based on number of classes so, the label set $L = [Water, Soil, Canopy]$ or considering detecting boundary, the label set $L = [Boundary, nonboundary]$ assigns a label to each value of $x$ on site $K$.
A random field regarding the neighbourhood system is a Markov Random Field (MRF) and it has the three following properties with respect to probability density function (Tso and Mather, 2009):

1) Positivity: $P(x) > 0$ for all possible configurations of $x$.
2) Markovianity: $P(x_r|x_{K-r}) = P\left(x_r|x_{N_r}\right)$, and
3) Homogeneity: $P\left(x_r|x_{N_r}\right)$ is the same for all sites $r$

where $K - r$ is the set difference that means all the pixels in the set $K$ except $r$, $x_{K-r}$ identified the set of labels at the sites in $K - r$, and $N_r$ is the neighbours of site $r$.
On the positivity as the first property of MRF, $P(x)$ can be calculated in practice by local conditional properties for all random fields. The second property which is markovianity means that labelling of a site $r$ is just depends on its neighboring sites $(N_r)$. The third property is homogeneity which means the conditional property of pixel $r$ given the labels from the neighboring pixels is not related to the position of site $r$ in $K$.
A Gibbs Random Field (GRF) is defined in terms of global properties unlike the MRF that provides a local property. In MRF, the label classes to each pixel is based on its neighbours whereas, in GRF the label class that assigned to each pixel is affected by all other pixels. Considering the joint distribution of classes for all pixels, the unique theory of GRF can be used for every MRF as a MRF-GRF equivalence (Tso and Mather, 2009). The probability density function in GRF is written as:

$$P(x) = \frac{1}{Z} exp\left[-\frac{U(x)}{T}\right] \tag{3.6}$$

where $U(x)$ is energy function, $T$ is a constant termed temperature and $Z$ is partition function which is written as:

$$Z = \sum exp\left[-\frac{U(x)}{T}\right] \tag{3.7}$$

where summation is carried over all possible configurations of $x$. $U(x)$ as a energy function in GRF contains number of cliques $(C)$ which are subsets. With respect to equation (3.6), it is obvious that by maximizing $P(x)$ the energy function is minimized. The energy function is written as:

$$U(x) = \sum_{c \in C} V_c(x) \tag{3.8}$$

where $V_c(x)$ is potential function regarding clique $C$.

In traditional classification techniques, label class is assigned to each pixel with respect to pixel value as a DN (Digital Number) value so, there is no any consideration along the contextual information. In MRF, a context is a prior information which be modelled by MRF. Furthermore, the Bayesian formula can utilize to construct the global energy. The conditional probability for Bayesian formula can be written as:

$$P(c_r|x_r) \propto P(x_r|c_r)P(x_r) \tag{3.9}$$

The posterior energy is defined:

$$U(c_r|x_r) = U(x_r|c_r) + U(x_r) \tag{3.10}$$

where $U(c_r|x_r)$ is posterior energy, $U(x_r|c_r)$ is conditional energy and $U(x_r)$ is prior energy.

### 4.1.3. Super Resolution Mapping

SRM used energy function as conditional probabilities of multispectral and panchromatic images to provide optimum result of labeling classes as canopy and soil. The method is applied in the GeoEye satellite image to providing a 0.5 $m$ resolution grape tree map. In this method, firstly, SRM provides a classified map at the finer spatial resolution from input image. During this process, because of mixed pixels the class label of each finer pixel is not clear.
Initial SRM of finer image $x$ classified with MRF neighbouring and that image get class $c(a_{i|j})$ as a label. $P(c)$ is prior probability and conditional probability is $P(y|c)$ in SR map. However, $P(c|y)$ is posterior probability. According to probability function energy function in GRF in Equation 3.6:

$$P(c) = \frac{1}{A_1} \exp\left[-\frac{U(c)}{T}\right] \tag{3.11}$$

$$P(y|c) = \frac{1}{A_2} \exp\left[-\frac{U(y|c)}{T}\right] \tag{3.12}$$

$$P(c|y) = \frac{1}{A_3} \exp\left[-\frac{U(c|y)}{T}\right] \tag{3.13}$$

$$P(q|c) = \frac{1}{A_4} \exp\left[-\frac{U(q|c)}{T}\right] \tag{3.14}$$

where $T$ is constant called temperature, $y$ is the multispectral image, $c$ is the super resolution map, $q$ is the panchromatic image, $A_i$, $i = 1, \dots, 4$ are normalization independent constant of $c$, $U(c)$ is prior energy, $U(y|c)$, $U(q|c)$ and $U(c|y)$ are conditional energies functions. According to equation 3.6, by eliminating independent terms as $c$, the energy function is written as:

$$U(c|y) = \lambda U_c(c) + (1-\lambda)(\lambda_{pan} U(q|c) + (1-\lambda_{pan}) U(y|c)) \tag{3.15}$$

where $\lambda$ is a smoothness parameter ($0 \le \lambda < 1$) that provides a balance for contribution of prior and conditional energy functions. $\lambda_{pan}$ as a smoothness parameter of panchromatic images ($0 \le \lambda_{pan} < 1$) provides the balance between two conditional energy between multispectral and panchromatic images of the GeoEye respectively (Ardila Lopez, 2012).

- **Simulated annealing**

When the posterior energy and optimized smoothness parameters were determined, an appropriate class label defines to each pixel for estimating Maximum a Posterior (MAP) by means of minimizing the posterior energy. It means that the standard against the pixel labelling is to find the MAP (Tso and Mather, 2009). Tso and Mather (2009) pointed out Simulated Annealing (SA) compare to other algorithms contains lowest energy, highest classification accuracy and it is very time consuming. In this research, the SA algorithm applied to find the MAP solution. SA is one of the stochastic algorithm based on probability statistics and random numbers. This algorithm includes the annealing parameters which are initial temperature $T_0$ and updating temperature $T_{upd}$ to control the randomness. Higher temperature means high randomness and low temperature denotes less temperature which means the high temperature enlarge the probability of labelling pixels by means of replacing new class and the energy of new class is higher (Kassaye, 2006). It means, from high temperature to low temperature the system is slowly cooled and frozen that means this process is repeated until the system becomes frozen (i.e. $T \rightarrow 0$). The iteration is repeated three times for each temperature update value and if the label of the pixel is not changed during the iteration the algorithm allow to finish the process (Tso and Mather, 2009).

- **Row-based approach**

To test the proposed methods on the prepared remote sensing data sets, the area of interest is divided into 28 rows which has the shared coverage in both GeoEye satellite image and UltraCam digital aerial photo (Figure 4.2). Moreover, the SRM grid is tiled using georeferencing to allocate the pixels of SRM and the images.

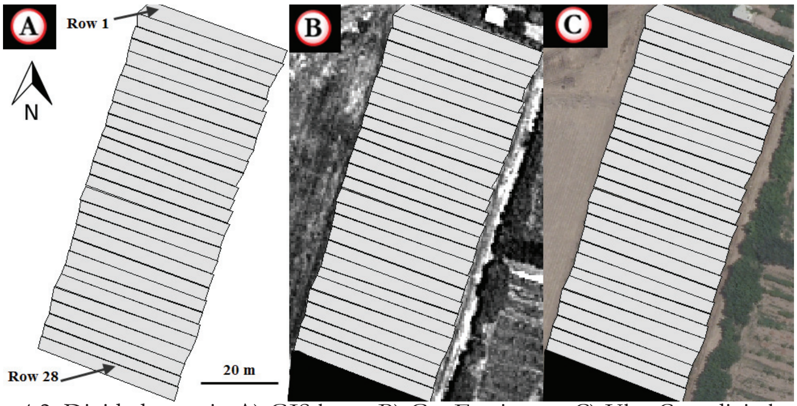


Figure 4.2: Divided rows in A) GIS layer, B) GeoEye image, C) UltraCam digital aerial photo

- **Plant-based approach**

For preparing a map of individual plants, visual interpretation based on the UltraCam aerial image and the panchromatic image of Geoeye applied to make a block for each plant and create a reference data for evaluating the result (Figure 4.3). It is important to note that this work is not possible to perform for some rows and plants. Because, some trees in rows are not pruned and there is an interlock between trees.

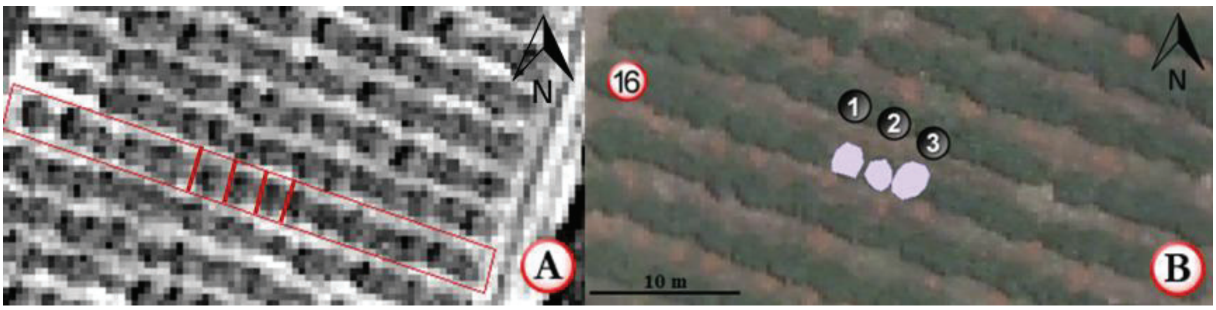


Figure 4.3: Creating blocks for each plant A) GeoEye panchromatic image B) Reference polygons in the aerial photo

## 4.2. Crop water requirement

EvapoTranspiration (ET) comprises to two simultaneous processes which are evaporation and transpiration. Evaporation is the process that water is lost from the soil surface and transpiration is occupied when the water is removed from the wet vegetation (Allen et al., 1998). There are two different prospects of evapotranspiration which are Actual ET (AET) and Potential ET (PET). AET is the process that water is eliminated from the surface with two separate processes which are evaporation and transpiration and, PET is the capability of the atmosphere to get rid of the water from the surface in consequence of evaporation and transpiration processes (Pidwirny, 2006). In agricultural irrigation management systems, it is important to distinguish how much additional water have needed for the crops to maximization of crop productivity. Crop water Requirement (CWR) identified by two important mentioned parameters as AET and PET (Pidwirny, 2006):

$$CWR = PET - AET \tag{3.16}$$

When the amount of AET is greater than PET, it means that the crop is irrigated extremely and, when the AET is less than PET there is water stress on the crop and it requires the water supplemental.

#### 4.2.1. Retrieved actual daily ET using SEBS model

The Surface Energy Balance System (SEBS) is a remote sensing model for assessing the daily EvapoTranspiration per pixel based on the resolution of the thermal band of image data (Su, 2002). SEBS utilizes satellite earth observation data such as MODIS, ASTER and Landsat satellite images with a combination of ground meteorological data as inputs for calculating the surface energy balance. Generally, SEBS requires three input sets of information (Figure 4.4):

1) The first set comprises of land surface emissivity, albedo, temperature and Normalized DiferenceVegetation Index (NDVI). These inputs can be derived from remote sensing data.
2) The second set contains air pressure, humidity, temperature and wind speed at reference height. The reference height is the measurement height like weather stations.
3) The third data set contains downward shortwave radiation and downward longwave radiation which can be measured directly or used output model.

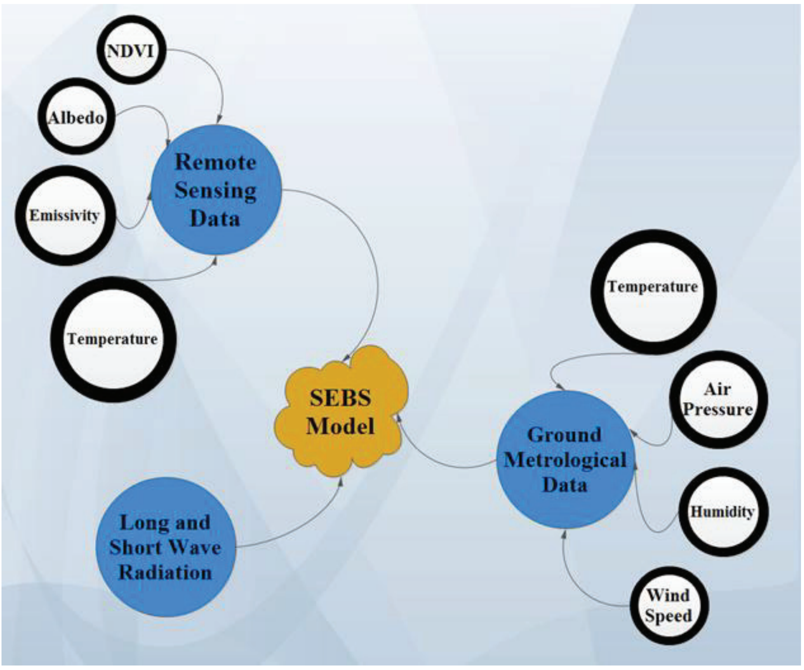


Figure 4.4: Three input data sets for the SEBS

The result of actual evapotranspiration is very sensitive to temperature, wind speed, vapour pressure and shortwave and longwave radiations (Aghdasi, 2010).

The surface energy balance is written as:

$$R_n = H + \lambda^* E + G_0 \tag{3.17}$$

where $R_n$ is the net radiation flux, $H$ is the sensible heat flux, $\lambda^* E$ is the latent heat flux and $G_0$ is the soil surface heat flux. The unit of each term of the energy balance system is $W\ m^{-2}$.

In this research, the SEBS model is applied to the Landsat 5 TM data to evaluate the daily ET and its applicability within the SRM. First, the raw data of each band from Landsat 5 TM converted to radiance and reflectance. Then, the SMAC (Simplified Method in the Atmospheric Correction) method (Rahman and Dedieu, 1994) was used for atmospheric correction of the Landsat 5 TM data. The Land Surface Temperature (LST) is taken from the thermal band of Landsat 5 TM using the method by (Sobrino et al., 2004). The Normalized difference Vegetation Index (NDVI) (Carlson and Ripley, 1997) is extracted from from red band and Near Infrared band of Landsat 5 TM.

The surface net radiation flux $(R_n)$ is estimated by incorporating of the retrieved surface emissivity, land surface temperature $(LST)$ and albedo from the Landsat 5 TM data and by the use of longwave and the surface solar radiation and surface thermal radiation downwards from the ECMWF (http://data-portal.ecmwf.int/data/d/interim_full_daily) data portal. The net radiation flux $R_n$ is estimated as:

$$R_n = (1 - \alpha).R_{swd} + \varepsilon.R_{lwd} - \varepsilon.\sigma.T_0^4 \tag{3.18}$$

where $\alpha$ is albedo, $R_{swd}$ is the downward solar radiation, $R_{lwd}$ is the downward longwave radiation, $\varepsilon$ is the surface emissivity, $\sigma$ is the Stefan Boltzmann constant ($5.7 \times 10^{-8}\ Wm^{-2}K^{-4}$) and $T$ is the air temperature at reference height ($K$).
The surface albedo for shortwave radiation ($\alpha$) is derived from narrowband to broadband convertion by Liang (Liang, 2001). The five bands of Landsat 5 TM is appropriate for calculating the surface albedo. The equation is written as:

$$\alpha = 0.356r_1 + 0.130r_3 + 0.373r_4 + 0.085r_5 + 0.072r_7 - 0.0018 \tag{3.19}$$

where $r_1, r_3, r_4, r_5$ and $r_7$ are the surface reflectance bands which are derived from the Landsat 5 TM bands 1, 3, 4, 5 and 7. The Land Surface Emissivity (LSE) is estimated from the the NDVI method by Sobrino (Sobrino et al., 2004) from the visible and near infrared bands of Landsat 5 TM regarding type of mixed pixels as the pixel depending on the NDVI values from the atmospheric correction..

The soil heat flux equation is:

$$G_0 = R_n[\Gamma_c + (1 - f_c).(\Gamma_s - \Gamma_c)] \tag{3.20}$$

where $f_c$ is the fractional canopy coverage, $\Gamma_c = 0.05$ is an empirical constant that related to the ratio of soil heat flux to net radiation for full vegetation canopy and $\Gamma_s = 0.315$ is for bare soil (Su, 2002).
The latent heat flux can be written as:

$$\lambda^{*}E = \Lambda(R_n - G_0) \tag{3.21}$$

Finally, the daily actual ET can be estimated as (Su, 2002):

$$ET_{daily} = 8.64 \times 10^{7} \times \Lambda_0^{24} \times \frac{\overline{R_n} - \overline{G_0}}{\lambda^{*}\rho_w} \tag{3.22}$$

where $ET_{daily}$ is the daily actual EvapoTranspiration $(mm\ day^{-1})$, $\overline{R_n}$ is the daily average of net radiation, $\lambda^{*}$ is the latent heat of vaporization $(\lambda^{*} = (2.501 - 0.00237 \times T_{air}) \times 10^{6})$, $\rho_w$ is the density of water $(1000\ kg\ m^{-3})$. In addition, the soil heat flux $\overline{G_0}$ is normally assumed for 24 hours.

#### 4.2.2. Estimating potential ET

In this study, it is assumed that the largest value of actual ET from the SEBS equals potential ET. Because of the absence of retrieving potential ET using RS data. There are some methods for determining potential ET with respect to meteorological data. One of the most famous methods is based on FAO Penman-Monteith which is described in section 4.4.2 to compare with the assumed maximum value using actual ET from the SEBS.

### 4.3. Image fusion for integration of actual ET and NDVI

Laben and Brower (2000) were developed the Gram-Schmidt Spectral Sharpening (GS) method. This method has been executed only in ENVI (Environment for Visualizing Image) software by $ITT^{®}$ (Ha et al., 2012)

In this research, GS method was applied to resample the result of AET from the SEBS as the lower resolution image with 30 $m$ spatial resolution using NDVI extracted from the GeoEye satellite image as the high resolution data with 50 $cm$ spatial ground resolution. In this study, it is assumed that the NDVI as high resolution image includes the vegetations which are contain higher AET estimated from the low resolution image which is daily AET from the SEBS. It means the pixel area which has the soil property is determined as the lower daily AET.

The GS method contains four steps in ENVI (Laben and Brower, 2000). In step 1, a coarser spatial resolution image is simulated and GS transformation is performed at step 2 on the simulated coarser resolution image. In step 3, the statistical information at finer spatial resolution image is adjusted compared to statistical information of the first transform GS to provide an adapted finer resolution image. In the final step, the inverse GS transformation is applied and then provide the enhanced spatial resolution image.

### 4.4. Validation

To decrease the uncertainty from the result of ET that obtained from the SEBS, the FAO Penman-Monteith methodology is used to estimate the the daily ET. Moreover, the result of SRM from each row and individual plants were evaluated by the use of UltraCam digital area photo and the panchromatic image of the GeoEye satellite image respectively.

#### 4.4.1. Generating reference data for validation of SRM

For evaluating the result of SRM, a reference map as the rows and individual plants used to assess the result of SRM. The UltraCam digital aerial photo and the panchromatic band of GeoEye satellite image utilized for creating the reference map for selecting rows and individual plants respectively. Figure 4.5

illustrates the reference polygons that are taken from the UltraCam aerial photo with respect to the panchromatic image of the GeoEye per row. This reference data applied to evaluate the result of SRM.

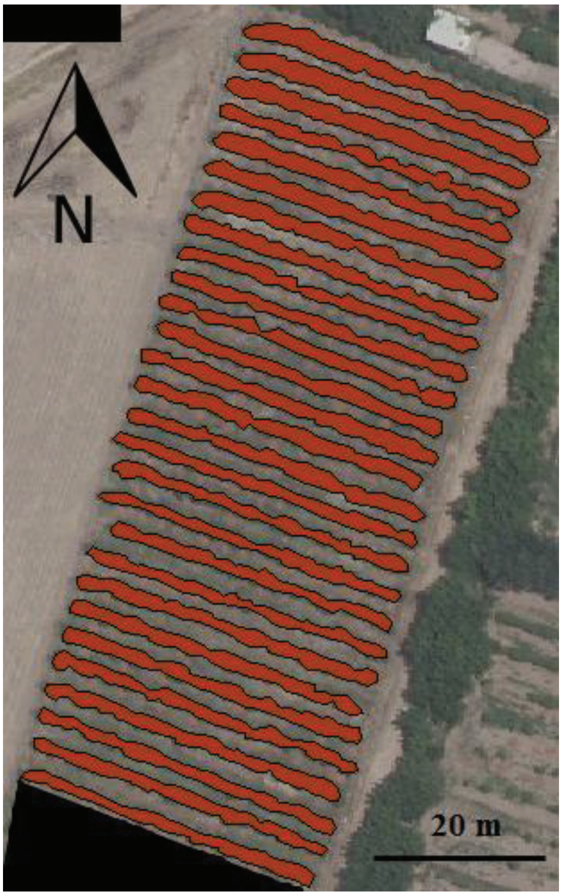


Figure 4.5: Reference polygons in digital aerial photo for assessing the result of SRM

After classification of SRM result, it is necessary to assess the accuracy of classification with respect to the reference data. The accuracy means how many pixels are classified in inside the polygon as reference considering the total classified pixels. Kappa coefficient is one the quality measurement that can be derived from the confusion matrix. Confusion matrix or error matrix represents user and producer accuracy. Producer accuracy means the relation between number of correct classified pixels in a polygon as the reference map and total number of the classified pixels. User accuracy is the probability of classified pixel that denotes information of class labels on the reference. Kappa coefficient indicates the overall agreement between reference polygons and classified map.

The range of kappa coefficient is between 0 and 1. Landis and Koch (1977) pointed out the relative strength of agreement for kappa coefficient. If the kappa coefficient equals 1 it means a perfect agreement with polygons as reference data. The value of 0.6 or higher means a substantial and good correlation. In this research, the result will be assessed in terms of kappa coefficient which measured the accuracy.

#### 4.4.2. Determining reference ET based on FAO Penman-Monteith

The uncertainty of estimated actual ET from the SEBS is generally comparable to ground measured ET (Su, 2002). Because of the absence of in-situ data, there is a standard method for determining reference crop EvapoTranspiration ($ET_0$) considering FAO Penman-Monteith equation (Allen et al., 1998) by the use of meteorological data. The amount of ET based on the FAO Penman-Monteith methodology is written as:

$$\mathrm{ET_c} = \mathrm{ET_0} \times \mathrm{K_c} \tag{3.23}$$

where $ET_c$ is the crop evapotranspiration under standard condition, $ET_0$ is reference crop evapotranspiration for grass as the reference crop and $K_c$ is the coefficient factor for the well watered crop in the optimal agronomic condition. The $K_c$ as a single crop coefficient of grape tree was chosen at middle season (based on Table 12 at FAO-56 (Allen et al., 1998)). The amount of $ET_0$ is determined as:

$$ET_0 = \frac{0.408\Delta(R_n - G) + \gamma\frac{900}{T+273}u_2(e_s - e_a)}{\Delta + \gamma(1 + 0.34u_2)} \tag{3.24}$$

where $R_n$ is the net radiation at the crop surface ($MJ\,m^{-2}\,day^{-1}$), $G$ is the soil heat flux density ($MJ\,m^{-2}\,day^{-1}$ ), $T$ is the air temperature at 2 $m$ height (℃), $u_2$ is the wind speed at 2 $m$ height ($m\,s^{-1}$), $e_s$ is the saturation vapour pressure ($KPa$), $e_a$ is the actual vapour pressure ($KPa$), $e_s - e_a$ is the saturation vapour pressure deficit ($KPa$), $\Delta$ is the slope vapour pressure curve ($KPa$ ℃$^{-1}$) and $\gamma$ is the psychrometric constant ($KPa$ ℃$^{-1}$).
In this study, because of the lack of potential ET from RS data, the maximum value of actual ET from the SEBS was assumed as the potential ET which is comparable with the amount of $ET_c$.

# 5. RESULTS

## 5.1. SRM result from the GeoEye satellite image

First of all, the result of SRM from the GeoEye image presents as a subset for detecting the rows. Then, some rows are taken as the row-based approach. Finally, with respect to the reference data and panchromatic image of the Geoye some individual plants extracted from a row.

### 5.1.1. Detecting rows

In this part, a subset of area of interest is taken from the GeoEye image which is included three rows. The aim of this part is to validate the result of SRM regarding the different parameter estimation. Despite the fact that we are interested in row detection so, two land cover classes as the canopy and soil are identified considering control the spectral mixing and also class mean and covariance matrices are estimated subsequently. These classes are recognized using feature space and visual interpretation. After parameter optimization, the best parameters are taken for detecting each row as a row-based and plant-based approaches. The scale factor equals four because, the aim of SRM result is to achieving finer spatial resolution image at 0.5 $m$ resolution. This subset includes three rows from row number 17 to row number 19. To apply the SRM based MRF the best parameter values are chosen to maximize the accuracy of row detection regarding the energy function (Equation 3.15). Table 5.1 indicates the best optimal parameters with respect to the high quality of row detection in the optimal SRM result obtained as $\kappa = 0.72$.

Table 5.1: Optimum parameters of SRM based MRF

| $T_0$ | $T_{upd}$ | $\lambda$ | $\lambda_{pan}$ |
|---|---|---|---|
| 3 | 0.9 | 0.9 | 0.4 |

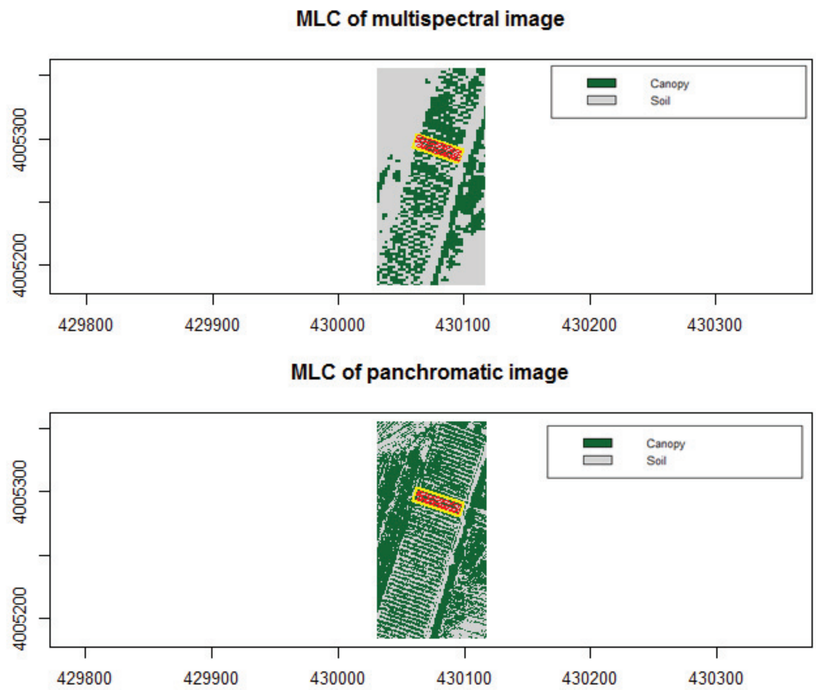


Figure 5.1: MLC result of panchromatic and multispectral images of the GeoEye data

Figure 5.1 illustrates the result of Maximum Likelihood Classification (MLC) with kappa 0.61. $T_0$ is initial temperature and $T_{upd}$ is a parameter for updating temperature in the simulated annealing algorithm. By raising the updating temperature value, the amount of iterations for assigning class labels is increased. Tolpekin and Stein (2009) recommended 0.9 for updating temperature because of time consuming and lowest energy in the SA algorithm that leads to fast classification computation. Based on agreement of accuracy, Lopez (2012) observed that the best quality of optimum SRM result based on tuning subset is reached with smoothness parameters which are 0.75 and 0.3 for multispectral and panchromatic images respectively and the kappa for these parameters reached 0.69. Regarding Table 5.1 and selecting smoothness parameters 0.9 for multispectral and 0.4 for panchromatic images, we observed the highest quality of agreement which is 0.72 as kappa coefficient. With these optimum parameters (Table 5.1), the lowest energy and optimum number of iterations are observed (Figure 5.2).

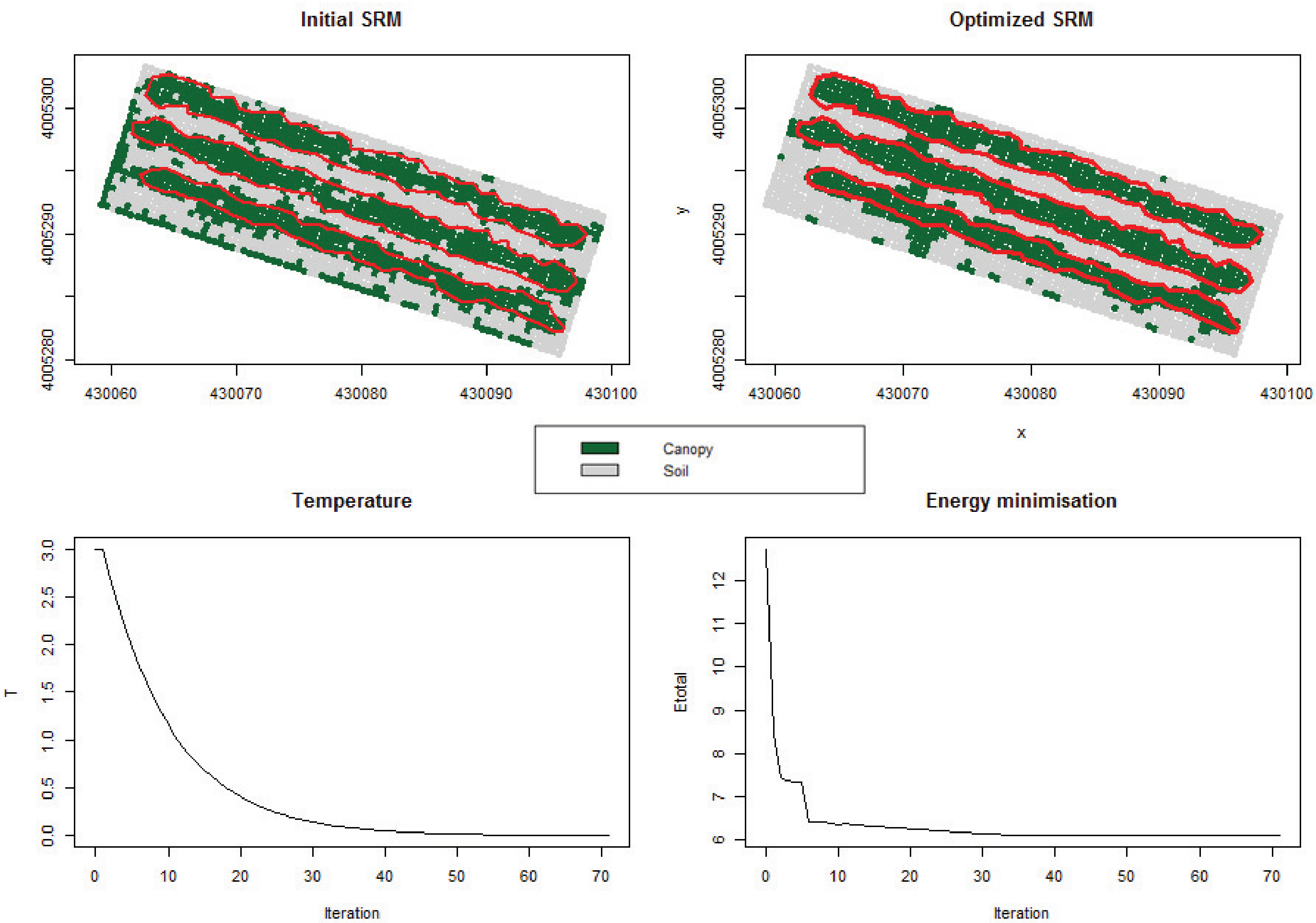


Figure 5.2: The result of SRM based MRF for the subset with S=4, $T_0$=3, $T_{upd}$=0.9, λ=0.9 and $\lambda_{pan}$=0.4

### 5.1.2. Rows within the field

After row detection in section 5.1.1, 10 rows from number 11 to number 21 were selected for applying SRM. For performing SRM, the optimum parameters from section 5.1.1 utilized to identify each row. Figure 5.3 illustrates the optimized result of SRM per row.

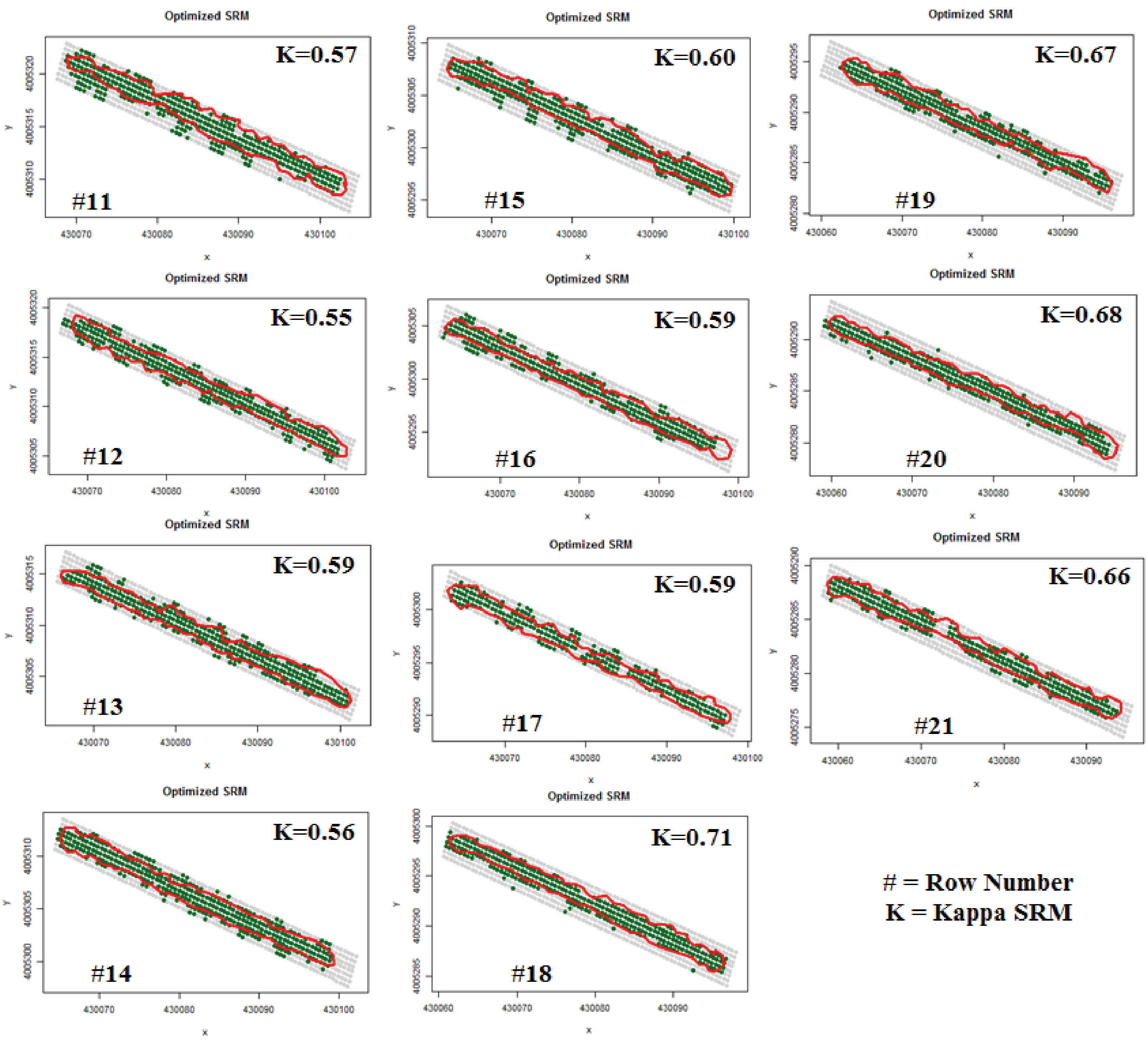


Figure 5.3: Result of SRM based MRF from row number 11 to row number 21

In this approach, each row is the input data as coarse resolution image. Based on optimum parameters in section 5.1.1, they are evaluated with kappa coefficient and then the number of canopy pixels is extracted per row for integration of using the SEBS.

### 5.1.3. Plants within the row

Three individual plants as reference polygons considered based on the proposed methodology in section 4.1.3. Figure 5.4 displays the result of initial and optimized SRM for three individual plants in row number 16. The parameters were chosen like the optimum parameters in section 4.1.1 for identifying these plants. The amount of $\kappa$ for three trees obtained as 0.64, 0.60 and 0.71 respectively.

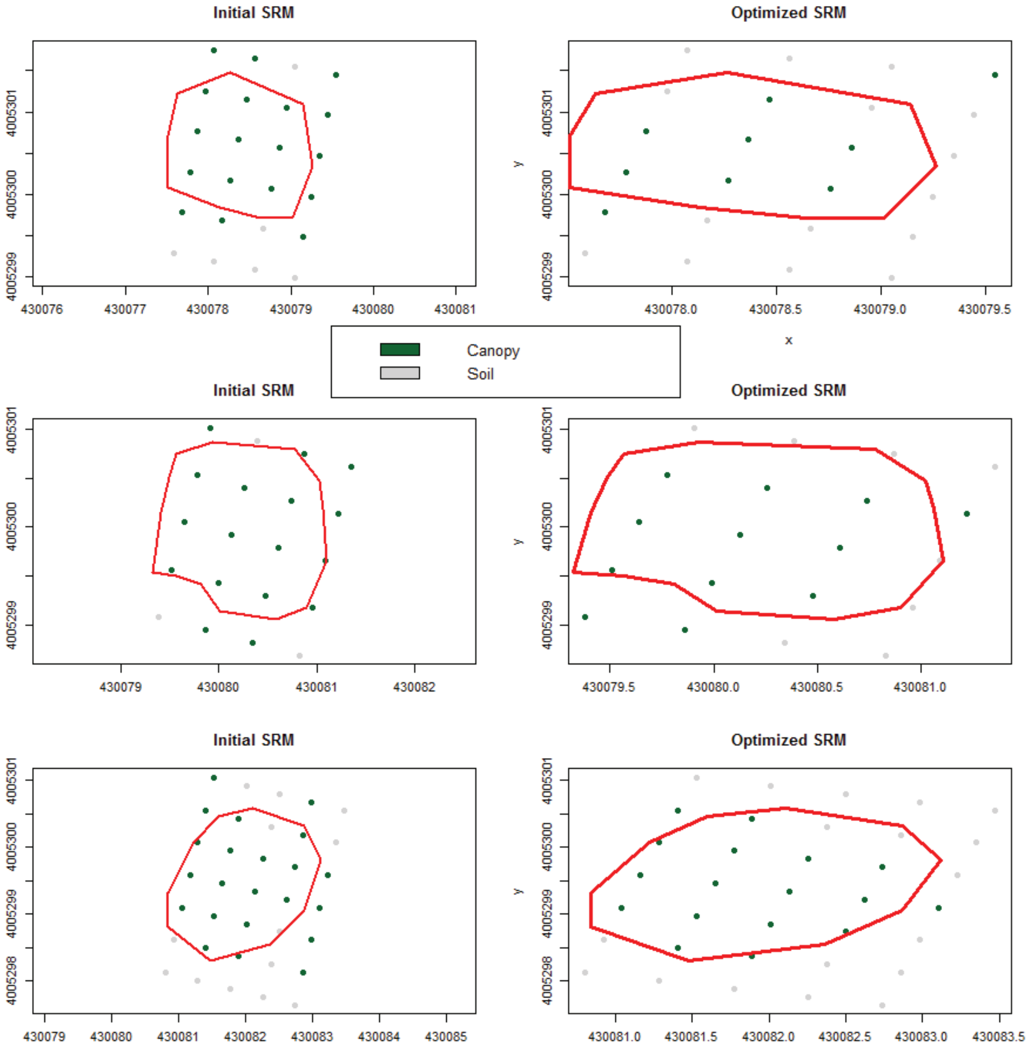


Figure 5.4: The result of SRM for individual plants in row number 16

Figure 5.4 shows that the optimum result of SRM include the smooth pixels in each individual plant with respect to the result of initial SRM. From tree number 1, the initial SRM took 18 pixels as canopy class, but the optimal SRM after SA consider 9 pixels. For tree number 2 and 3 these amount of pixels are from 17 to 12 and form 22 to 17 respectively.

## 5.2. Daily ET result from the Landsat 5 TM satellite image

The result of actual evapotranspiration around the area of interest from the RS data and SEBS is indicated in Figure 5.5. The SEBS calculates the AET per pixel and the resolution of each pixel originates from the resolution of LST which estimated by Landsat 5 TM thermal infrared band. It means the resolution of AET equals 30 $m$ per pixel with respect to the resolution of the LST.

The retrieval result of actual daily ET from the SEBS as a maximum value is 5.76 $mm\ day^{-1}$ around the area of interested and it was assumed as the potential ET. This value is compared to the amount of potential ET which is 5.71 $mm\ day^{-1}$ based on the FAO Penman-Monteith methodology in section 4.4.2.

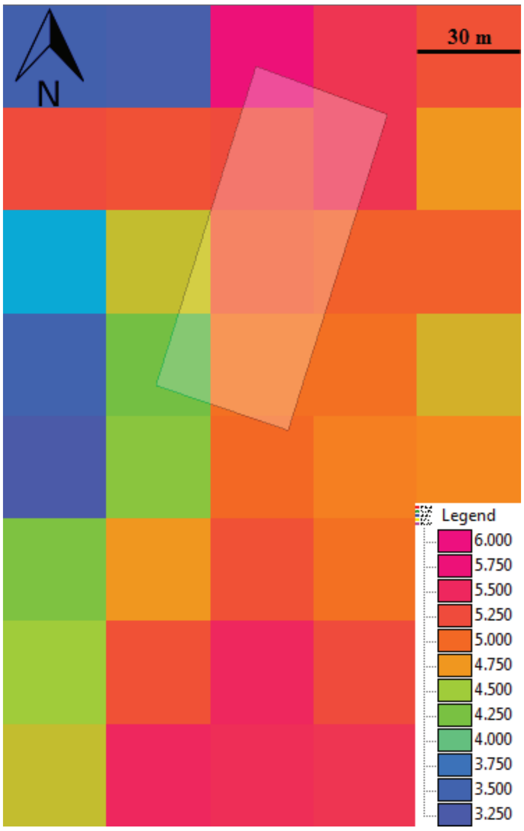


Figure 5.5: The result of retrieval actual daily ET based on the SEBS around the area of interest

## 5.3. Image fusion between actual ET and NDVI maps

In this part, the Gram-Schmidt (GS) method utilized for applying image fusion between an actual ET image from the SEBS and NDVI map of the GeoEye image. The image which contains the actual ET with 30 meter resolution is indicated as a coarse resolution image and the NDVI map with 0.5 $m$ resolution is considered as a high resolution image. It is assumed that the NDVI as vegetation index which shows the live vegetations can be fused with the actual ET image in terms of vegetations include the higher actual ET and the rest of the area which covered by soil embraces the lower actual ET. With this assumption, it could be possible to perform the image fusion. Figure 5.6 shows the result of image fusion using the GS method.

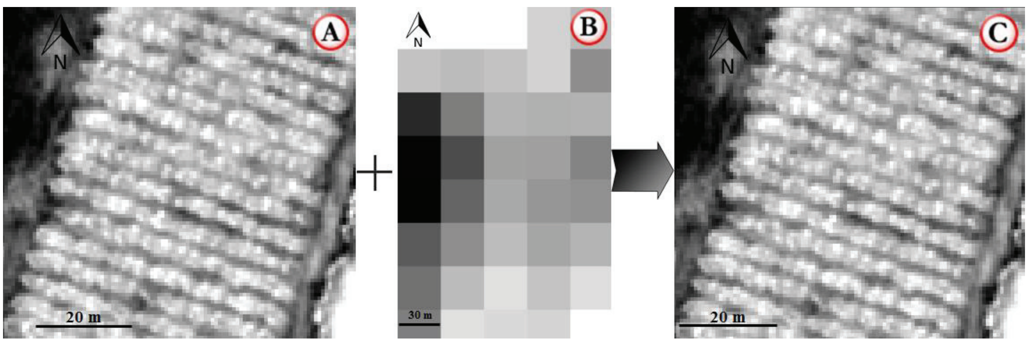


Figure 5.6: Result of (C) image fusion between (B) actual ET image and (A) NDVI image using the GS method

## 5.4. Application of SRM and SEBS for precision agriculture

The aim of this part is to show the application of SRM for precision agriculture. First of all, the relation between SRM result and actual ET per row and individual plant displays. Then the specification of NDVI map as vegetation index indicates for rows and individual plants.

### 5.4.1. Allocating the ET value per rows and individual plants

In this part, the result of SRM with 0.5 $m$ resolution per row and individual plants allocating to fused image which includes the actual ET with 0.5 $m$ resolution from section 5.3. Figure 5.7 illustrates the actual ET in a row number 18 and three individual plants in row number 16 respectively.

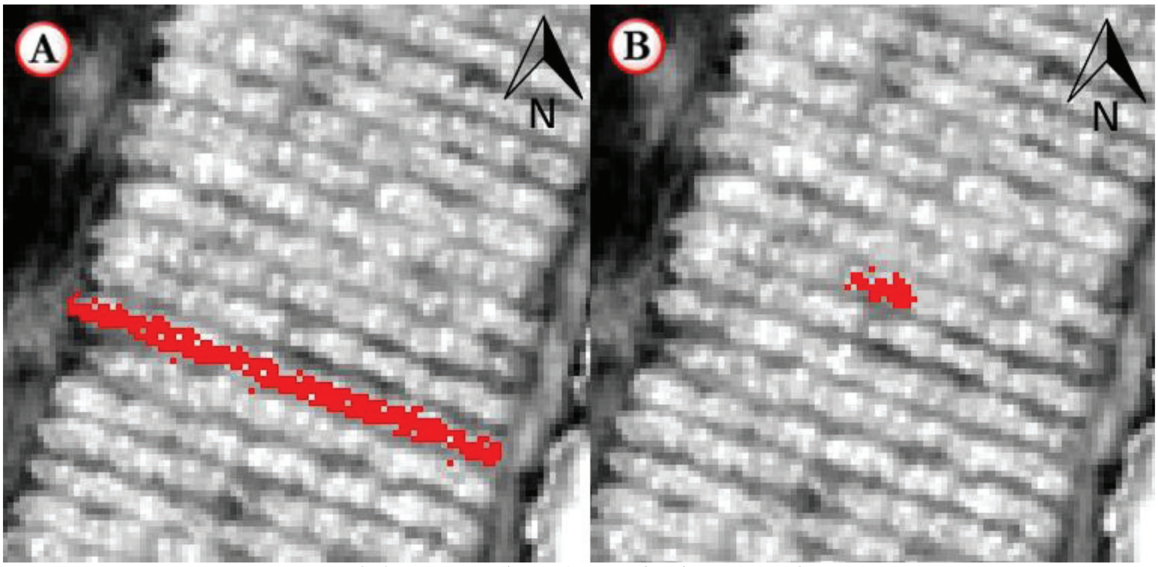

Figure 5.7: SRM result of (A) a row and (B) three individual plants for allocating actual ET

Table 5.2 indicates the result of actual ET for row number 18 and three individual plants in row number 16 respectively. For assigning actual ET for each row or individual plant the mean value per pixels was considered.

Table 5.2: Result of actual ET in row number 18 and three individual plants in row number in row 16

| Row number and Individual Plants | Actual ET |
|---|---|
| 18 | 5.34 |
| 16_1 | 5.29 |
| 16_2 | 5.33 |
| 16_3 | 5.36 |

### 5.4.2. Specifying the NDVI per rows and individual plants

It is useful for farmers who want to know the information regarding the health of each plant. Because, NDVI as a vegetation index required to control at any agricultural field. Hence, by the use of SRM result per row and plant scale and combining that result with 0.5 $m$ resolution per pixel and the NDVI map with 50 $cm$ resolution, every farmer will be able to control the health of vegetations. Figure 5.8 displays the combination of SRM and the NDVI per row and individual plants. For allocating NDVI value for each row and plants, the mean value was considered.

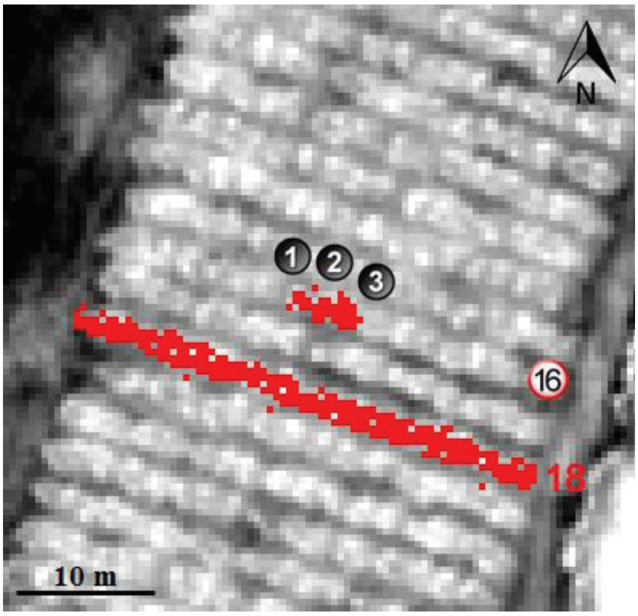


Figure 5.8: Combination of SRM result with NDVI for row number 18 and three plants of row number 16

Table 5.3: NDVI value for row number 18 and three individual plants in row number 16

| Row number and Individual Plants | NDVI |
|---|---|
| 18 | 0.49 |
| 16_1 | 0.49 |
| 16_2 | 0.49 |
| 16_3 | 0.50 |

# 6. DISCUSSION

In this chapter, the result of SRM based MRF and actual ET from the SEBS in chapter 5 addresses and then the applicability of using SRM and the SEBS is discussed in detail to support the crop water requirement in precision agriculture.

For implementing SRM based MRF, the set of training pixels as the canopy and soil are chosen in both multispectral and panchromatic bands. There was a limitation for selecting land cover classes in the multispectral image of the GeoEye; because of the absence of variation between soil and canopy pixels. So, for choosing training pixels as the soil, an area close to the area of interest was selected. Hence, the result of Jeffery-Matusita spectral class separability was confirmed for the two defined classes. Then, for the input image in SRM we decided to select an appropriate scale factor value (Tolpekin and Stein, 2009). The scale factor identifies the neighbourhood window size based on Equation 3.5. In this study, the scale factor equals four because of integration between the SEBS and SRM. Based on the scale factor, each pixel of SRM result has 0.5 $m$ spatial resolution. Moreover, for detecting rows in the area of interest, a small subset of three rows was chosen and based on  indicator that was presented by Lopez (2012) optimum smoothness parameters of SRM selected. There are other parameters for SRM that demonstrates the quality of SRM as smoothness ($\lambda$) parameters, class separability (Tolpekin and Stein, 2009), initial temperature ($T_0$) and parmeter for updating temperature ($T_{upd}$) (Sepehri, 2011). The initial SRM obtained class labels randomly per pixel and because of the noisy result, smoothness parameters have a main role to provide a smoother optimum SRM result. Regarding Equation 3.15 in section 4.1.3, smoothness parameter controls the relation between likelihood and prior energy for energy minimization and determine a balance in the energy equation (Equation 3.15). Tolpekin and Stein (2009) pointed out that the optimum smoothness parameter for different scale factor in synthetic image is not the same. Lopez (2012) observed that the optimum $\lambda$ and $\lambda_{pan}$ for the best quality in real data are 0.75 and 0.3 respectively. In this research, the optimum value of smoothness parameters based on the maximum kappa coefficient value which is 0.72 estimated as 0.9 and 0.4 for detecting rows. If $\lambda_{pan}$ equals zero, it means that the information of panchromatic image is ignored (Ardila Lopez, 2012). For assigning class labels to each pixel, simulated annealing was applied (section 4.1.3) during the iterations until getting frozen point. Initial temperature ($T_0$) controls the simulated annealing algorithm. Sepehri (2011) tested values of 0 and 3 for initial temperature ($T_0$) and observed that selecting $T_0 = 3$ leads to the result of initial SRM randomly reduce the iteration and using 0 value for initial SRM cannot be selected randomly in the synthetic image. In our results the initial temperature equals 3 and $T_{upd}$ is 0.9. Choosing the updating temperature about 0.9 updated the pixels and changed their classes during the 63 iterations compare to $T_{upd} = 0.95$ by 174 iterations took the long time computation. Kassaye (2006) recommended values 0.8 and 0.9 for updating temperature as optimal values for simple and complex scene respectively. These parameters were considered for applying SRM based MRF for row-based approach in section 4.1.3. The important reason in this study for achieving low accuracy is due to the reference data, which is the UltraCam digital aerial photo. Because, the time of acquisition of the GeoEye image and aerial photo is more than a year and some changing during the growing season could be effected on selecting an appropriate boundary for each row and individual plants. Lopez (2012) obtained the maximum kappa for four subsets of urban trees as the optimal SRM result which are 0.73, 0.67, 0.68 and 0.54. We observed maximum kappa which are 0.64, 0.60 and 0.71 in section 5.1.3 for three subsets of individual plants respectively. After a row-based approach and extracting individual plants, the plants and rows were extracted to linking  the SRM result and actual ET for supporting precision agriculture.

The result of actual ET from the RS data was obtained using SEBS around the area of interest. Ma (2012b) compared the result of actual ET from Landsat 5 TM and the SEBS with in-situ measurements and observed a small difference between them. In this study, because of the lack of in-situ data we could not compare the result of actual ET to decrease the uncertainty of the SEBS. Just a maximum value of the actual ET around the area of interest was assumed as the potential ET because of the absence of retrieving potential ET from the RS data. The maximum actual ET value equals 5.76 $mm\,day^{-1}$ and it was allocated as a potential ET. On the other hand, the potential ET was calculated based on the Penman-Monteith methodology in section 4.4.2 and using ground meteorological data and it equals 5.71 $mm\,day^{-1}$. The difference between these two values is small. So, the maximum value of actual ET using the SEBS was taken for potential ET for estimating crop water requirements for each row and individual plants. Water requirement of agricultural field is not always fixed and deterministic. The water stress at any particular position in the field or region shows variations. Characterization of variability depends on temporal, spatial and weather-related categories (Vintila et al., 2012). Besides differences in weather information, there is an effect on the variation on result of actual ET during the growing season. In many production situations, such as grape trees in a vineyard area only one type of crop is cultivated. At each crop growing season there is variation in temperature, solar radiation, humidity and other weather data whereas estimation of actual evapotranspiration information is sensitive on these data.

- **Integration of SRM and SEBS to support precision agriculture**

An important problem for linking the SEBS and SRM result is connecting the resolution of RS images. The Geoeye provides high spatial resolution satellite images and on the other hand, Landsat 5 TM produces medium spatial resolution images. To overcome this problem, image fusion using Gram-Schmidt (GS) method applied to increase the spatial resolution of the actual ET image from 30 $m$ resolution to 0.5 $m$ spatial resolution equivalent to the resolution of the SRM result. For performing this method, the NDVI image from pansharpened GeoEye image utilized for down-scaling. It was assumed that vegetation in the NDVI map represents a higher actual ET with respect to the soil, with smaller actual ET.
The crop water requirement is identified in section 4.2. If the actual ET value exceeds the potential ET then, this means that the crop is irrigated. But, if the potential ET value exceeds the actual ET, there is water stress for crops. Based on Table 5.2, for row number 18 and individual plants in row 16 the amount of actual ET is 5.34, 5.29, 5.33 and 5.36 $mm\,day^{-1}$ respectively. It means that all of the grape trees in row number 18 and individual plants in row number 16 have an actual ET below the potential ET which is 5.76 $mm\,day^{-1}$. So, there is water stress on these crops and plants have to be irrigated e.g. using irrigation network.

- **End product to support the irrigation networks and precision agriculture**

Precision agriculture aims at providing management strategy from multiple sources to support the decision makers and farm managers with crop production (Oliver, 2010) using advanced technologies in Geomatic science such as integration RS, GIS and GPS data.
In this study, the water requirement was the main issue for farmers and decision makers. Decision maker or the farmer who wants to make a plan or strategy for irrigation networks of agricultural fields can use the applicability of RS data by running the SEBS on the basis of SRM. This product helps farmers and decision makers to decide on the amount of water requirements to maximize the cost benefit ratio of crop productivity. The application of using the SEBS on the basis of SRM provides the crop water requirement at the plant scale vineyard to support precision agriculture. This product provides a map of actual evapotranspiration and NDVI per row and plants to develop the farm management strategies on irrigation networks. It means that farmer and decision makers can utilize these maps per row or individual plants to assess the crop stress using NDVI and crop water requirement by the use of the actual evapotranspiration

map. At the end, they can utilize a strategy to how to optionally irrigate the area and select those irrigation methods that are appropriate to use and to make a plan for fertilization based on the NDVI map.

- **Limitations**

In this research, limitations undoubtedly exist. The below list shows several shortcoming limitations during this study:

- Lack of ASTER image (ASTER SWIR data acquired since April 2008 are not usable) for the possibility of comparing retrieval actual ET from different satellite resolution and different sensors.
- Absence of in-situ data for the retrieval actual ET result validation.
- Lack of variation in the multispectral bands of the GeoEye image for taking training pixels.
- Absence of complete weather information near the study area for meteorological data using the SEBS.
- No possibility of field works to evaluate the observations
- Absence of buildings around the field regarding taking ground control points for georeferencing the UltraCam digital aerial photo
- Different time of acquiring between the GeoEye and Ultracam aerial photo for creating the reference data

# 7. CONCLUSION AND RECOMMENDATIONS

The main objective of this study is to explore the possibility of assessing the crop water requirement using SRM and the application of SEBS. It includes the following sub-objectives:

1. To estimate the actual and potential ET at plant scale vineyard using SRM and the application of SEBS.
2. To assess applicability of integrated the SEBS and SRM.
3. To determine the quantity of water requirement at plant scale using fusion technique.

In order to address the objectives of this research, five research questions were formulated. Several methods carried out using RS data sets regarding to answer the posed questions. In chapter 5, the achieved results presented and in chapter 6, the results were discussed. In this chapter, we present a conclusion of this research on the basis of the perspective of the research questions. Then, limitation of the research will be presented and regarding the findings during the research some recommendations will be given for further research.

## 7.1. Conclusion

This study was undertaken to explore the possibility of integration using the SEBS and SRM for assessing the crop water requirement at plant scale. In this section, the research questions and corresponding answers are addressed:

1. Which satellite images are appropriate as spatial resolution to support SRM for extracting information on individual plants?
Detection of rows in the field and extracting information on individual grape trees in vineyard requires the use of high resolution images. The reason is that SRM based MRF uses information of both spatial and spectral of RS data to assign class labels to the pixels. There is spatial and spectral variation that can be obtained from low and medium satellite images useable at the plant scale.

2. What could be the role of SRM at plant scale information for vineyard?
Traditional classification methods consider spectral information of images. SRM helps to increase the resolution of the classification result obtained from a coarse resolution input image. MRF as a contextual classification method considers both spectral and spatial information data to deal with mixed pixels. Using SRM leads to a smoother result as compared to the use of classifiers, like the k-NN or maximum likelihood classifiers.

3. How to extract information of individual plants at vineyard using SRM?
For extracting information on individual plants, each plant was extracted as a block in the row by using visual interpretation and used as input to a coarse resolution image for performing SRM. The digital aerial photo and the panchromatic image of satellite images were used to ensure that each block contained one plant. Then, with SRM based MRF the optimum SRM result of plants was observed. Furthermore, the quality of agreement was assessed using kappa coefficient.

4. How to validate the result of SRM?
To decrease the uncertainty, the result of optimum SRM for each row and individual plant were evaluated using digital aerial photo with respect to the panchromatic image of the GeoEye image by creating the

reference map. For assessing the SRM result, we used kappa coefficient that denotes the overall accuracy between a classified SR map and a reference polygon.

5. How to integrate the SEBS and SRM?
We applied the Gram-Schmidt image fusion for retrieval of actual ET using the SEBS with 30 $m$ resolution as the low resolution image and a NDVI map of the GeoEye image with 0.5 $m$ resolution as the high resolution image. It was assumed that the NDVI image reflects that vegetation that has a higher actual ET as compared to the soil. The actual ET map was obtained at a 0.5 $m$ resolution and could be used for integration with the SRM ET and NDVI at a 0.5 $m$ resolution.

## 7.2. Recommendations

This research presents the role of remote sensing data to retrieve actual ET using the SEBS and SRM for the crop water requirement at the plant scale vineyard and extract information of grape trees. One of the problems regarding make a link between these two approaches related to the low and medium coarse resolution satellite images like MODIS, ASTER and Landsat. On the other hand, absence of thermal infrared and middle infrared bands in high resolution RS data is obvious. To improve the applicability of RS data for irrigation network at the plant scale vineyard, the shortcoming recommendations for further researches address as following:

1. Combine high resolution satellite image with digital aerial photo for improving the result of SRM at plant scale. It means, improve the multispectral image of high resolution satellite images using image fusion is necessary to test the result of SRM method.

2. Using different fusion techniques to assess the quality of image fusion using NDVI and actual ET maps.

3. Besides using the SEBS for retrieving actual ET, it is possible to extract such the other information like Leaf Area Index (LAI) from the SEBS for contributing other applications in precision agriculture.

4. Applying different time of satellite images during a year or growing season (temporal) to determine the water deficit and provide a meaningful product for the farmer and decision makers to make a strategic plan for irrigation networks.

5. Using and developing Object-oriented SRM modelling and provide a model (not pixels) on the basis of a certain shape of the canopy for extracting individual plants.

## 7.3. Future work

- **Integration of Low, Medium and High Resolution Satellite Data to Support Real Time Water Supply Strategies for Farm Management**

Precision agriculture aims at providing the management strategy from multiple sources to support the decision makers and farm managers with crop productions (Oliver, 2010). It supports assessment, management and evaluation of space-time in crop production and how to handle variation in diverse level

of detail that never before reached; and achieve the level of quality that never before obtaining correctly (Pierce and Nowak, 1999). All these questions have to be answered in an environment, with plenty of uncertainty related to adoption of proper policy on available techniques in agricultural area (Zhang et al., 2002). Precision agriculture needs "Timely", "Updated" and "Localized" information that was not available before such as "Optimal Control" of irrigation water (Vintila et al., 2012). As an example, Farmers require weekly info regarding crop and soil moisture conditions during the growing season. Remote Sensing (RS) technology produces data from processes that are taking place on the earth in variety types, and resolutions. Satellite data can be divided into three different general products such as high resolution, coarse resolution (low resolution) and medium resolution. There are many coarse resolution products that are publicly available and easy to obtain and use in many applications. Higher resolution images have a high spatial resolution but lacking diverse spectral resolution such as middle infrared and thermal bands which are used for retrieving evapotranspiration, water content, leaf area index and other products necessary for precision agriculture. Fusion approaches can be carried out to produce a relevant RS product using high, medium and low resolution images. By means of the application of remote sensing technologies, satellite images such as the high spatial resolution images can be used to identify trees and to study spatial characteristics. However, application of coarse spatial resolution with high temporal and spectral resolution in farm managements is problematic, as they have a large pixel size that is not very useful for management at the farm level. This problem can be solved by means of fusion techniques. To produce the timely and localized end products, image fusion could be combined the high temporal and high spatial resolution satellite data in combination with high spatial resolution satellite data to produce proper information such as timely crop water requirement useful for farm management. Water requirement of agricultural field is not always fixed and deterministic. The water stress at any particular position in the field or region shows a variation. Characterization of variability depends on temporal, spatial and weather-related categories. Besides of differences in weather data have an effect on the variation during the growing season. In many production situations, such as grape trees in a vineyard area only one type of crop is cultivated. At each crop growing season there is variation in temperature, solar radiation, humidity and other factors of the weather data. These variations are in contrast with temporal and spatial variation (Oliver, 2010). For a farmer who needs the information on water demands at any plant scale during the next few days, it is possible to provide a geostatistical model to predict the water supplements. Satellite images like Senitel that observe every location on the earth every five days. By the use of remote sensing data, and a proper geostatistical model, the farmer can provide the predicted weather data for the next coming days at the plant level and get the appropriate information with respect to the crop water requirement.
In this context, this research concept is aimed at achieving the following three objectives:

1. Define a model with contribution of Super Resolution technique that can support identification of plants using medium and high resolution satellite data.
2. Support down-scaling of low and medium scale publicly available RS products and produce high resolution thematic data useful for precision agriculture and using image fusion technique.
3. Integrate and apply these two methods to support real time water supply strategies of the farm.

# LIST OF REFERENCES


Abkar, A. & Fatemi, S. 2004. Application of a GIS as a modeling tool for remote sensing image analysis of agricultural fields.

Abkar, A. A., Sharifi, M. A. & Mulder, N. J. 2000. Likelihood-based image segmentation and classification: a framework for the integration of expert knowledge in image classification procedures. *International Journal of Applied Earth Observation and Geoinformation,* 2**,** 104-119.

Aghdasi, F. 2010. *Crop Water Requirement Assessment and Annual Planning of Water Allocation.* MSc, Faculty ITC, Twente University.

Allen, R. G., Pereira, L. S., Raes, D. & Smith, M. 1998. Crop evapotranspiration-Guidelines for computing crop water requirements-FAO Irrigation and drainage paper 56. *FAO, Rome,* 300**,** 6541.

Allen, R. G., Tasumi, M. & Trezza, R. 2007. Satellite-based energy balance for mapping evapotranspiration with internalized calibration (METRIC)—Model. *Journal of irrigation and drainage engineering,* 133**,** 380-394.

Ardila Lopez, J. P. 2012. *Object - based methods for mapping and monitoring of urban trees with multitemporal image analysis.* University of Twente Faculty of Geo-Information and Earth Observation (ITC).

Atkinson, P. M. 2009. Issues of uncertainty in super-resolution mapping and their implications for the design of an inter-comparison study. *International Journal of Remote Sensing,* 30**,** 5293-5308.

Bastiaanssen, W., Menenti, M., Feddes, R. & Holtslag, A. 1998. A remote sensing surface energy balance algorithm for land (SEBAL). 1. Formulation. *Journal of Hydrology,* 212**,** 198-212.

Boucher, A. & Kyriakidis, P. C. 2006. Super-resolution land cover mapping with indicator geostatistics. *Remote Sensing of Environment,* 104**,** 264-282.

Brisco, B., Brown, R., Hirose, T., Mcnairn, H. & Staenz, K. 1998. Precision agriculture and the role of remote sensing: a review. *Can J Remote Sens,* 24**,** 315-327.

Carlson, T. N. & Ripley, D. A. 1997. On the relation between NDVI, fractional vegetation cover, and leaf area index. *Remote Sensing of Environment,* 62**,** 241-252.

Dowman, I., Jacobsen, K., Konecny, G. & Sandau, R. 2012. High Resolution Optical Satellite Imagery.

Fisher, P. 1997. The pixel: a snare and a delusion. *International Journal of Remote Sensing,* 18**,** 679-685.

Foody, G. M. 2006. Sub-pixel methods in remote sensing. *Remote sensing image analysis: Including the spatial domain***,** 37-49.

Ha, W., Gowda, P. H. & Howell, T. A. 2012. A review of potential image fusion methods for remote sensing-based irrigation management: part II. *Irrigation Science***,** 1-19.

Haglund, A. 2000. Towards soft classification of satellite data. *A case.*

Hu, R. & Fahmy, M. M. 1992. Texture segmentation based on a hierarchical Markov random field model. *Signal processing,* 26**,** 285-305.

Kalma, J. D., Mcvicar, T. R. & Mccabe, M. F. 2008. Estimating land surface evaporation: a review of methods using remotely sensed surface temperature data. *Surveys in Geophysics,* 29**,** 421-469.

Kasetkasem, T., Arora, M. K. & Varshney, P. K. 2005. Super-resolution land cover mapping using a Markov random field based approach. *Remote Sensing of Environment,* 96**,** 302-314.

Kassaye, R. H. 2006. Suitability of Markov random field-based method for super-resolution land-cover mapping. *Master dissertation, International Institute for Geo-information Science and Earth Observation.*

Laben, C. A. & Brower, B. V. 2000. Process for enhancing the spatial resolution of multispectral imagery using pan-sharpening. Google Patents.

Landis, J. R. & Koch, G. G. 1977. The measurement of observer agreement for categorical data. *Biometrics***,** 159-174.

Li, S. Z. 2009. *Markov random field modeling in image analysis*, Springer.

Liang, S. 2001. Narrowband to broadband conversions of land surface albedo I: Algorithms. *Remote Sensing of Environment,* 76**,** 213-238.

Luo, R. & Kay, M. 1992. Data fusion and sensor integration: State-of-the-art 1990s. *Data Fusion in Robotics and Machine Intelligence***,** 7-135.

Ma, W., Hafeez, M., Ishikawa, H. & Ma, Y. 2012a. Evaluation of SEBS for estimation of actual evapotranspiration using ASTER satellite data for irrigation areas of Australia. *Theoretical and Applied Climatology***,** 1-8.

Ma, W., Hafeez, M., Rabbani, U., Ishikawa, H. & Ma, Y. 2012b. Retrieved actual ET using SEBS model from Landsat-5 TM data for irrigation area of Australia. *Atmospheric Environment.*

Mahour, M. & Abkar, A. A. 2012. Evaluation of Model Based Image Analysis of Remotely Sensed Data Using Support Vector Machine and Bayes' Theorem. Tehran, Iran: International Conference of Geomatics 91.
Menenti, M. & Choudhury, B. 1993. Parameterization of land surface evaporation by means of location dependent potential evaporation and surface temperature range.
Mertens, K., Verbeke, L., Ducheyne, E. & De Wulf, R. 2003. Using genetic algorithms in sub-pixel mapping. *International Journal of Remote Sensing,* 24**,** 4241-4247.
Muad, A. & Foody, G. 2010. Super-Resolution Mapping of Landscape Objects from Coarse Spatial Resolution Imagery. *ISPRS Journal,* XXXVIII-4/C7.
Oliver, M. A. 2010. *Geostatistical applications for precision agriculture*, Springer.
Pidwirny, M. 2006. "Actual and Potential Evapotranspiration". *Fundamentals of Physical Geography, 2nd Edition.*
Pierce, F. J. & Nowak, P. 1999. Aspects of precision agriculture. *Advances in agronomy,* 67**,** 1-85.
Pohl, C. & Van Genderen, J. 1998. Review article Multisensor image fusion in remote sensing: concepts, methods and applications. *International Journal of Remote Sensing,* 19**,** 823-854.
Rahman, H. & Dedieu, G. 1994. SMAC: a simplified method for the atmospheric correction of satellite measurements in the solar spectrum. *REMOTE SENSING,* 15**,** 123-143.
Richards, J. A. 2012. *Remote sensing digital image analysis: an introduction*, Springer.
Roerink, G., Su, Z. & Menenti, M. 2000. S-SEBI: A simple remote sensing algorithm to estimate the surface energy balance. *Physics and Chemistry of the Earth, Part B: Hydrology, Oceans and Atmosphere,* 25**,** 147-157.
Sarkar, A., Biswas, M. K., Kartikeyan, B., Kumar, V., Majumder, K. & Pal, D. 2002. A MRF model-based segmentation approach to classification for multispectral imagery. *Geoscience and Remote Sensing, IEEE Transactions on,* 40**,** 1102-1113.
Sepehri, N. 2011. *Super Resolution Mapping with Support Vector Machine.* University of Twente.
Sobrino, J. A., Jiménez-Muñoz, J. C. & Paolini, L. 2004. Land surface temperature retrieval from LANDSAT TM 5. *Remote Sensing of Environment,* 90**,** 434-440.
Su, Z. 2002. The Surface Energy Balance System (SEBS) for estimation of turbulent heat fluxes. *Hydrology and Earth System Sciences Discussions,* 6**,** 85-100.
Tatem, A., Lewis, H., Atkinson, P. & Nixon, M. 2003. Increasing the spatial resolution of agricultural land cover maps using a Hopfield neural network. *International Journal of Geographical Information Science,* 17**,** 647-672.
Tatem, A. J., Lewis, H. G., Atkinson, P. M. & Nixon, M. S. 2001. Super-resolution target identification from remotely sensed images using a Hopfield neural network. *Geoscience and Remote Sensing, IEEE Transactions on,* 39**,** 781-796.
Thomopoulos, S. C. A. 1990. Sensor integration and data fusion. *Journal of Robotic Systems,* 7**,** 337-372.
Tolpekin, V. A., Ardila, J. P. & Bijker, W. 2010. Super-resolution mapping for extraction of urban tree crown objects from VHR satellite images. *Small,* 3**,** 1.
Tolpekin, V. A. & Stein, A. 2009. Quantification of the effects of land-cover-class spectral separability on the accuracy of Markov-random-field-based superresolution mapping. *Geoscience and Remote Sensing, IEEE Transactions on,* 47**,** 3283-3297.
Tso, B. & Mather, P. 2009. *Classification methods for remotely sensed data*, CRC.
Tso, B. & Olsen, R. C. 2005. A contextual classification scheme based on MRF model with improved parameter estimation and multiscale fuzzy line process. *Remote Sensing of Environment,* 97**,** 127-136.
Verhoeye, J. & De Wulf, R. 2002. Land cover mapping at sub-pixel scales using linear optimization techniques. *Remote Sensing of Environment,* 79**,** 96-104.
Vintila, R., Lazar, C., Poenaru, V., Radnea, C. & Voicu, P. 2012. A first reference spatial remote sensing and agronomic knowledge base for precision agriculture and related applications. *Stiinta Solului– Soil Science, XLVI (1),??-??.*
Vrabel, J. 1996. Multispectral imagery band sharpening study. *Photogrammetric Engineering and Remote Sensing,* 62**,** 1075-1084.
Wang, L., Parodi, G. & Su, Z. SEBS Module BEAM: A Practical Tool for Surface Energy Balance Estimates from Remote Sensing Data. 2008.
Wu, B., Yan, N., Xiong, J., Bastiaanssen, W., Zhu, W. & Stein, A. 2012. Validation of ETWatch using field measurements at diverse landscapes: A case study in Hai Basin of China. *Journal of Hydrology.*
Zhang, N., Wang, M. & Wang, N. 2002. Precision agriculture—a worldwide overview. *Computers and electronics in agriculture,* 36**,** 113-132.

Zhuang, X. Y., Shi, R. H. & Liu, C. S. Data fusion of satellite remotely sensed images and its application in agriculture.  Society of Photo-Optical Instrumentation Engineers (SPIE) Conference Series, 2011. 28.